Elastic theory of layered beams

Markku Heinisuo

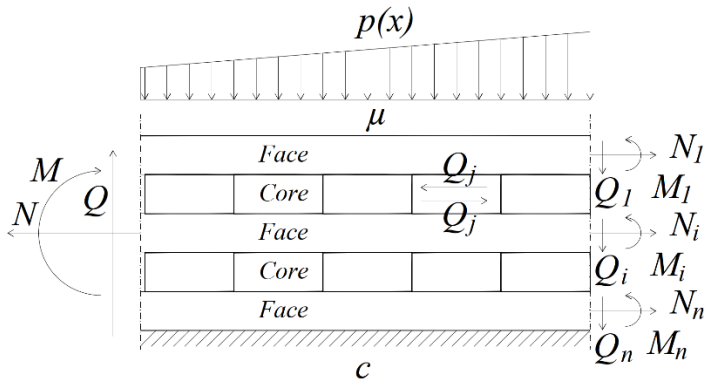

Tampere University, 2022

ISBN 978-952-03-2414-8 (pdf)

Forewords

The classical theory of layered beams is presented in details. The theory has been presented originally in 1940's to the design of composed wooden structures. Discussion of the basic assumptions is given in order to estimate the validity of the theory in different cases. Different formulations of the boundary conditions are presented. Some analytic solutions are given. These solutions are used in numerical examples. Summaries of recently presented cases of cross-laminated timber (CLT) beams and steel-timber composite beams are given including validation of the theory against experimental researches done by others. It is seen that the theory seems to be useful in estimation of the behaviour of these rather novel innovative structures. So far the theory has been used in the standards of sandwich and steel structures, but it seems to be suitable for possible future standards of CLT and steel-timber composite structures, as the theory was originally developed for wooden structures.

Contents

Introduction

In this paper is presented the theoretical background of the elastic theory of layered beams. The theories have been developed since 1940's to the analysis of different structures such as shown in Figure 1.

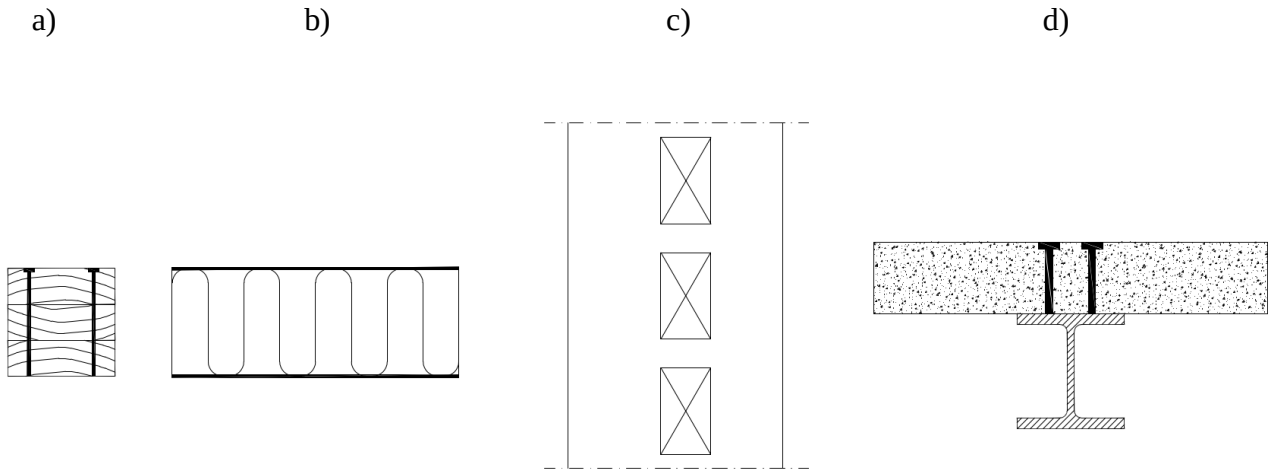

Figure 1. Layered beams.

In [Parland, 1942], [Granholm, 1949] and [Pleskov, 1952] the focus was in nailed wooden beams, Figure 1 a). Pleskov introduced a Generalized Bernoulli's hypothesis for the layered beams. This means that the centroids of the faces, which carry the axial loads in bending, stay at the line. This assumption is true for example to the beams which cross-sections consists of two faces and for the symmetric cross-section with three faces. Only axial deformations in the longitudinal axis of the beam are considered for the faces. The faces are connected by the cores and only shear deformations in the longitudinal axis of the beam are considered for those. In the nailed wooden beams the wooden boards are acting as the faces and the nails are acting as the cores. The method where the Generalized Bernoulli's hypothesis is not fulfilled leads to the group of differential equations which can be solved numerically [Rosman, 1965], [Itani & Hiremath, 1980].

In [Hoff & Mautner, 1948] was considered bending and buckling of sandwich beams, Figure 1 b). In sandwich beams the sheets (steel, aluminum, wood,…) of the surfaces are acting as the faces and the insualation (mineral wool, polyurethane etc) between the faces is acting as the core. The theory of the layered beams has been used most widely in the analysis of the sandwich structures [Stamm &

Witte, 1974], [Davies, 2001]. The basic equations of design, which are based on the theory of the layered beams, have been presented in the standard of sandwich structures [EN 14509, 2013].

In [Chitty, 1947] shear walls, Figure 1 c), were studied. In the shear walls longitudinal beams are acting as the faces and lintel beams are acting as the cores. The theory of shear walls is included in many standards, such as uniform built-up compression members in [EN 1993-1-1, 2005].

The beam theory which is suitable for example for composite beams including shear deformations, Figure 1 d), was given in [Timoshenko, 1921]. Later such as Gamma method [Möhler, 1956] and Shear analogy [Kreuzinger, 1999] have been presented. Gamma method is presented in many standards [EN 1995-1-1, 2004] and handbooks [Schickhofer et al, 2010], [Borgström & Fröbel, 2019] of timber structures and Shear analogy is presented in Canadian [Gagnon & Pirvu, 2011] and US [Karacabeyli & Douglas, 2013] handbooks of cross-laminated timber (CLT). In [Heinisuo & Pajunen, 2021] has been shown that the the group of differential equations of Gamma method leads to a sixth order differential equation, which is the basis of the elastic theory of layered beams, which is in the scope of this paper.

An approximate finite element method (FEM) was derived for layered beams in [Thompson et al, 1975]. This FEM uses a cubic splines for the lateral deflections of the beam and trapezoidal splines for the axial displacements of the faces. This ensures that the FEM coverges to the exact solution when the lengths of the finite elements are reduced. The exact finite element method formulations (the term “direct-stiffness method” is used in [Clough & Penzien, 1975] instead of the term “exact FEM”) for the layered beams are given in [Heinisuo, 1989] and in [Davies, 2001]. The general purpose finite element programs are widely used to the analysis of the layered beams, but they are not in the scope of this study.

The focus of this study is on the analytical methods. The key points of the theory are given following [Heinisuo, 1989]. Some recents results are given dealing with wooden structures including the comparisions against empirical results.

Kinematics and axial stresses of faces

The cross-section of the uniform beam consists of the faces i (i = 1, …, n) and the cores j (j = 1, …, n-1). The cross-section properties of the faces are the area A_i, the moment of inertia I_i and the Young’s

modulus E_i. The faces and the cores follow the Hooke' law. The deflection of the beam is denoted as $v(x)$ along the beam axis x. The main research question is to define the equations which are needed to define the deflection $v(x)$.

The beam is loaded with the lateral load $q(x)$ along the beam axis in y-direction, see Figure 1, and with the uniform tensile axial force N. The lateral load is decomposed into outer loading intensity $p(x)$, the reaction of the Winkler type foundation $-cv(x)$ where c is the foundation parameter and the inertia force $-\mu d^2v(x,t)/dt^2$ according to D'Alembert's principle and μ is the mass/length of the beam. We consider only the harmonic vibration so $q(x) = p(x) - cv(x) - \mu\omega^2 v(x)$, where ω is the angular velocity.

Consider the deformed face i. The angle φ is the rotation (positive clockwise) of the beam measured at the centroids of the faces, see Figure 2. The deflection of the beam is v and the longitudinal axis is x. The shear deformation of the faces is assumed to be negligible so the rotation of the faces is v' where the prime denotes differentiation with respect to x. The angle γ measures the slip between the centroids of the faces.

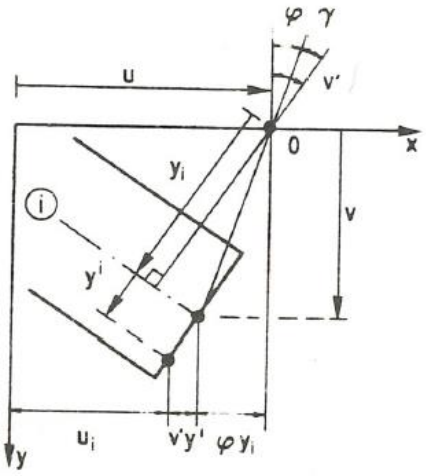

Figure 2. Displacement of the face i.

Referring to Figure 2 the equation

$$\varphi = v' - \gamma \tag{1.1}$$

is valid. Let u be the longitudinal dispalecement of a certain reference point O, y^i is the coordinate in the local centroidal coordinate system and y_i is the coordinate of the centroid of the face i. The longitudinal displacement of the face i is

$$u_i = u - y^i v' - y_i \varphi \quad i = 1, \dots, n. \tag{1.2}$$

The strain ε_i is

$$\varepsilon_i = u_i' = u' - y^i v'' - y_i \varphi' \quad i = 1, \dots, n. \tag{1.3}$$

From the Hooke's law follows that the axial stress σ_i of the face is

$$\sigma_i = E_i \varepsilon_i = E_i u' - E_i y^i v'' - E_i y_i \varphi' \quad i = 1, \dots, n. \tag{1.4}$$

The axial force N_i of the face i is defined as

$$N_i = \int_{A_i} \sigma_i dA_i = E_i A_i u' - y_i E_i A_i \varphi' \quad i = 1, \dots, n. \tag{1.5}$$

The bending moment M_i of the face i is defined as

$$M_i = \int_{A_i} \sigma_i y^i dA_i = -E_i v'' \int_{A_i} y^i y^i dA_i = -E_i I_i v'' = -B_i v'' \quad i = 1, \dots, n, \tag{1.6}$$

where $E_i I_i = B_i$ is the bending stiffness of the face i. The stress resultant N is defined as

$$N = \int_A \sigma_i dA = \sum_{i=1}^n N_i, \tag{1.7}$$

where the integration is performed over the area $A = \sum A_i$. Using Eq. (1.5) we get

$$N = \sum_{i=1}^n E_i A_i \, u' - \sum_{i=1}^n y_i E_i A_i \, \varphi' = EAu' - \sum_{i=1}^n y_i E_i A_i \, \varphi' \tag{1.8}$$

denoting the axial stiffness as

$$EA = \sum_{i=1}^n E_i A_i. \tag{1.9}$$

The centroid of the layered beam is defined as that point at which if $u' = 0$ then $N = 0$. From Eq. (1.8) follows

$$\sum_{i=1}^{n} y_i E_i A_i = 0 \Rightarrow\ y_i = \sum_{m=1}^{i-1} \left(\frac{E_m A_m}{\sum_{i=1}^{n} E_i A_i} \sum_{j=m}^{i-1} a_j \right) - \sum_{m=i+1}^{n} \left(\frac{E_m A_m}{\sum_{i=1}^{n} E_i A_i} \sum_{j=i}^{m-1} a_j \right), \quad (1.10)$$

where the distances of the adjacent centroids of the faces are

$$a_j = y_{i+1} - y_i. \quad (1.11)$$

The axial force *N* is then

$$N = EAu'. \quad (1.12)$$

The stress resultant *M* is

$$M = \int_A \sigma_i y dA = \sum_{i=1}^{n} \int_{A_i} \sigma_i \left(y_i + y^i \right) dA_i = \sum_{i=1}^{n} y_i N_i + \sum_{i=1}^{n} M_i, \quad (1.13)$$

or

$$M = M_s + M_0, \quad (1.14)$$

where the sum of the bending moments of the faces is $M_0 = \sum M_i$ and M_s is the bending moment of the axial forces

$$M_s = \sum_{i=1}^{n} y_i N_i = -\sum_{i=1}^{n} y_i^2 E_i A_i \varphi' = -B_s \varphi'. \quad (1.15)$$

The total bending stiffness *B* is defined as

$$B = B_s + B_0,\ B_0 = \sum_{i=1}^{n} B_i. \quad (1.16)$$

Using Eq. (1.1) the moment *M* is

$$M = -B_0 v'' - B_s (v'' - \gamma') = -B v'' + B_s \gamma'. \quad (1.17)$$

Consider next point C of the core *j* with the local coodinate $y^{i,C}$. The longitudinal displacement of point C is calculated from face *i*

$$u_{i,C} = u - y^{i,C} v' - y_i \varphi, \quad (1.18)$$

and it is assumed that there is no axial deformation of the core. When the displacement is calculated from the face i+1 then the result is

$$u_{i+1,C} = u - y^{i+1,C}v' - y_{i+1}\varphi. \tag{1.19}$$

The difference between these displacements is

$$u_{i+1,C} - u_{i,C} = -\left(y^{i+1,C} - y^{i,C}\right)v' - (y_{i+1} - y_i)\varphi = (y_{i+1} - y_i)\gamma \tag{1.20}$$

taking into account Eq. (1.1) and because the equation

$$y^{i+1,C} + y_i = y^{i,C} + y_i \tag{1.21}$$

is true. Using $a_j = y_{i+1} - y_i$, see Eq. (1.11) and denoting

$$\Delta_j = u_{i+1,C} - u_{i,C}, \tag{1.22}$$

the equation

$$\Delta_j = a_j\gamma \tag{1.23}$$

can be written. The slip Δ_j measures the slip at the core at the level of C, but according to Eq. (1.23) it is calculated as the difference of axial displacements at the centriods of the adjacent faces.

Using Eqs. (1.4), (1.12), (1.6) and (1.15) the axial stress of the face can be calculated as

$$\sigma_i = \frac{E_i}{EA}N + \frac{E_i y^i}{B_0}M_0 + \frac{E_i y_i}{B_s}M_s. \tag{1.24}$$

Consider next the shear forces and stresses.

Shear forces and stresses

The longitudinal shear flow T_j of the core is defined as

$$T_j = k_j\Delta_j = k_j a_j\gamma, \tag{2.1}$$

where k_j is the shear stiffness intensity of the core j. Consider the free body of the face i, see Figure 3. The shear force of the face is Q_i and q_i^j is the lateral loading intensity at the core j and y_j denotes the mid-point or the inflexion point of the core.

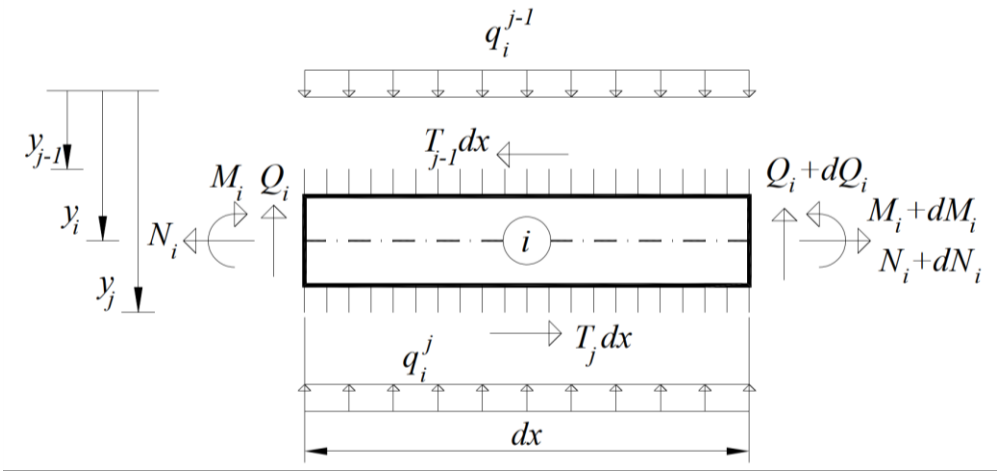

Figure 3. Free body of face.

The equilibrium equations of the differential free body give

$$Q_i' = q_i^j - q_i^{j-1}, (j = i), \tag{2.2}$$

$$N_i' = T_{j-1} - T_j, (j = i), \tag{2.3}$$

$$Q_i = M_i' + T_j(y_j - y_i) + T_{j-1}(y_i - y_{j-1}), (j = i). \tag{2.4}$$

By assuming that there is no longitudinal surface loading $T_0 = T_n = 0$ summation of equations (2.4) gives

$$Q = \sum_{i=1}^{n} Q_i = \sum_{i=1}^{n} M_i' + \sum_{j=1}^{n-1} a_j T_j. \tag{2.5}$$

The faces are acting as Bernoulli-Euler beams so $M_i = -E_i I_i v''$ and the shear flow T_j is following (2.1), then

$$Q = -\sum_{i=1}^{n} E_i I_i v''' + \sum_{j=1}^{n-1} a_j^2 k_j \gamma = Q_0 + Q_s = -B_0 v''' + k\gamma, \tag{2.6}$$

where is used the following definition for the shear factor k

$$k = \sum_{j=1}^{n-1} a_j^2 k_j. \tag{2.7}$$

The shear stress τ_j of the core j is

$$\tau_j = \frac{T_j}{b_j} = \frac{k_j a_j}{b_j}\gamma, j = 1, \dots, n-1 \quad , \tag{2.8}$$

where b_j is the width of the core j. The maximum value of the component τ_i of the shear stress of the face i is, assuming the parabolic shear stress distribution over the face

$$\tau_i = \frac{1.5Q_i}{A_i}, i = 1, \dots, n. \tag{2.9}$$

The shear stress distribution in the cross-section of the layered beam is presented in Figure 4 for the cases where the faces and the cores have the same width $b_j = b_i$, (j = 1, …, n - 1).

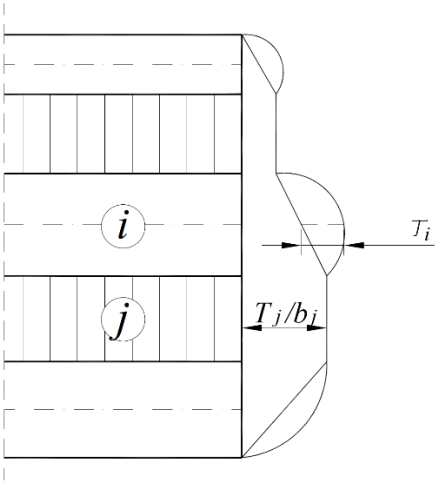

Figure 4. Shear stress distribution of the layered beam.

Short summary

As a summary can be stated that if the diplacement $v(x)$ and the rotation $\gamma(x)$ are known then the stress resultants can be calculated as

$$B = B_0 + B_s, \tag{2.10}$$

$$B_0 = \sum_{i=1}^{n} B_i = \sum_{i=1}^{n} E_i I_i, \tag{2.11}$$

$$B_s = \sum_{i=1}^{n} y_i^2 E_i A_i, \tag{2.12}$$

$$M(x) = M_0(x) + M_s(x), \tag{2.13}$$

$$M_0(x) = -B_0 v''(x), \tag{2.14}$$

$$M_s(x) = -B_s[v''(x) - \gamma'(x)], \tag{2.15}$$

$$Q(x) = Q_0(x) + Q_s(x), \tag{2.16}$$

$$Q_0(x) = -B_0 v'''(x), \tag{2.17}$$

$$Q_s(x) = k\gamma(x), \tag{2.18}$$

and the axial stresses using Eq.(1.24) and the shear stresses using Eqs. (2.8) and (2.9). The shear factor *k* is calculated using Eq. (2.7). The stress resultants are shown in Figure 5.

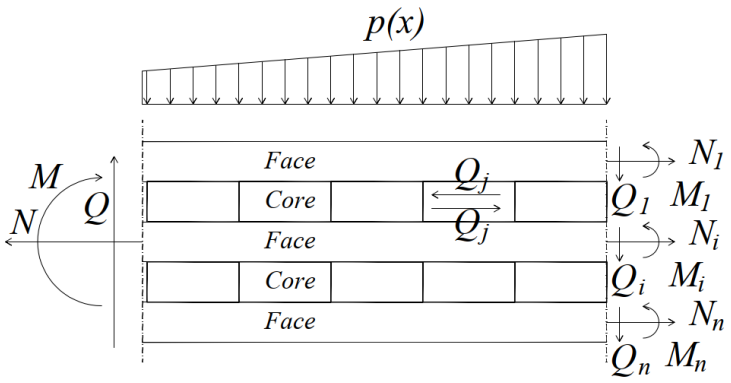

Figure 5. Stress resultants.

Periodical and sandwich cores

If the core is periodic, period l_j, then the shear force Q_j of the connector (lintel) can be calclated using the equation

$$Q_j = T_j l_j = k_j a_j l_j \gamma = \frac{k_j a_j l_j Q_s}{k}. \tag{3.1}$$

If there is only one core then

$$Q_1 = \frac{l_1}{a_1} Q_s. \tag{3.2}$$

The shear stiffness of one connector of the periodic core is k_s and then the shear stiffness intensity is

$$k_j = \frac{k_s}{l_s}. \tag{3.3}$$

If there is one core, i.e. two faces, then for the periodic core

$$k = \frac{k_s a_1^2}{l_s}. \tag{3.4}$$

Consider the sandwich core with a uniform shear stress τ_s and with the shear modulus G_j then

$$\tau_s = \frac{T_j}{b_j} = G_j \gamma_j \; and \; \Delta_j = \gamma_j h_j, \tag{3.5}$$

where h_j is the height of the core. In this case, compare Eq. (2.1)

$$k_j = \frac{G_j b_j}{h_j} => k = \frac{G_1 b_1 a_1^2}{h_1}, \tag{3.6}$$

and the last is valid for sandwich beams. If the faces are very thin $a_j \approx h_j$ then

$$k = G_1 b_1 h_1. \tag{3.7}$$

When there are two faces then the coordinates of the centroids of the faces are

$$y_1 = -\frac{E_2 A_2}{E_1 A_1 + E_2 A_2} a_1, \quad y_2 = \frac{E_1 A_1}{E_1 A_1 + E_2 A_2} a_1, \tag{3.8}$$

and from these can be defined the location of the origo.

Discussion of the theory

In this theory it is assumed that the core is continuous so that longitudinal shear stresses are also present at the boundary of core *j* and face *i* for all positions *x* of the beam, see Figure 4. As a result of this there are also longitudinal shear stresses τ_{si} at the faces. When the theory is used for

periodically connected beams, such as nailed beams or shear walls, then it is suggested that the shear stresses of the faces are only calculated by using Eq. (2.9) [Rosman, 1965].

The theory leads to disagreement between the equilibrium equations (2.3). Because the axial load N is a constant it follows from Eqs. (2.3), (1.5) and (2.1)

$$-y_i E_i A_i \varphi'' = \left(k_{j-1}a_{j-1} - k_j a_j\right)\gamma \Rightarrow y_i E_i A_i (v''' - \gamma'') = \left(k_j a_j - k_{j-1}a_{j-1}\right)\gamma, j = i. \qquad (4.1)$$

This equation states that the term $y_i E_i A_i/(k_j a_j - k_{j-1} a_{j-1})$ should be a constant. On the otherhand by summation of Eqs. (2.3) from index $j + 1$ to index n the longitudinal shear force T_j is

$$T_j = -\sum_{s=j+1}^{n} N_s' = \sum_{s=j+1}^{n}\left(y_s - y_j\right)E_s A_s (v''' - \gamma'') = S_j (v''' - \gamma''), \qquad (4.2)$$

and the definition of the modified static moment of section S_j can be seen in the previous equation. By comparing this equation with Eq. (2.1) it can be seen that the term $S_j/(k_j a_j)$ should be a constant. It can be seen that using Eq. (1.10) that if the terms $y_i E_i A_i/(k_j a_j - k_{j-1} a_{j-1})$ are a constant then the terms $-S_j/(k_j a_j)$ are the same constant, so this term can be considered as a measure for estimating the validity of the theory. These requirements are fulfilled if the beam is made of two faces and one core or three faces and two cores but the cross-section of the beam is symmetrical. The requirements are fulfilled also in some other special cases. In the general case the equilibrium equations are satisfied only approximatively.

The theories proposed by Parland and Pleskov differ from the present theory in respect of the contribution of the shear factor of the layered beam k in Eq. (2.7). Parland proposed [Parland, 1972] the following for this parameter

$$k = \frac{I_s^2}{\sum_{j=1}^{n-1} \frac{S_{js}^2}{k_j}}, \qquad (4.3)$$

where it is assumed that all the faces have the same modulus of elasticity and

$$I_s = \sum_{i=1}^{n} y_i^2 A_i, \qquad (4.4)$$

and the static moment is

$$S_{j,s} = \sum_{s=j+1}^{n}\left(y_s - y_j\right)A_s. \qquad (4.5)$$

According to Pleskov [Pleskov, 1952] it is assumed that all shear stiffness intesities are same $k_j = k^*$, then the shear factor is

$$k = \frac{k^*(n-1)B_S}{EA_r}, \tag{4.6}$$

where

$$EA_r = \sum_{j=1}^{n-1} \frac{S_j}{a_j}, \tag{4.7}$$

which can be derived by calculating the mean of Eqs. (4.2).

It is seen from Eqs. (2.7), (4.3) and (4.6) that all three theories include some limitations. All three theories gives indentical values if the equations

$$\frac{I_S}{\sum_{j=1}^{n-1} S_{js}^2} = \frac{n-1}{A_r} = \frac{\sum_{j=1}^{n-1} a_j^2}{I_s} \tag{4.8}$$

are valid. This case occurs for axmple in the situation where the ratios between the heights of the faces h_{i+1}/h_i are constant. Similar special cases can be found in other situations too and these cross-sections can be considered as those whose centroids stay always on the lone i.e. the Generalized Bernoulli's hypothesis is valid.

In [Heinisuo, 1989] are compared the results using all three theories and the results of the FEM [Thompson et al, 1975]. The FEM mesh was refined so that the values calculated were obtained to five significant digits. No clear recommendations of using three theories, present, Parland or Plaskov, could be given. The theory presented here is mainly recommended for use for analysing beams which fulfill the Generalized Bernoulli's hypothesis i.e. the terms $y_iE_iA_i/(k_ja_j\text{-}k_{j\text{-}1}a_{j\text{-}1})$ are a constant.

Differential equations and boundary conditions

The differential equations for the equilibrium of layred beams can be derived by considering the equilibrium equations of the differential free body of the beam or condering the stationarity condition of the total potential energy of the beam. Using the latter method the boundary conditions can also be derived, and it is used in this study. It is well-known that the complementarity in the boundary

conditions guarantees the existence of a unique soluton to the problem with the linear elasticity. The total potential energy Π of the elastic structure is [Langhaar, 1962]

$$\Pi = U + V, \tag{5.1}$$

where U is the strain energy and V is the potential of the loading. In this case the strain energy stored in the structure consists of the strain energy stored in the faces (only axial stains are considered) and the strain energy stored in the cores (only shear strains are considered). The following equation

$$U = \frac{1}{2}\int_0^L \sum_{i=1}^{n} \int_{A_i} \sigma_i \varepsilon_i dA_i dx + \frac{1}{2}\int_0^L \sum_{j=1}^{n-1} T_j \Delta_j \, dx = \frac{1}{2}\int_0^L [EAu'^2 + B_0 v''^2 + B_s(v'' - \gamma')^2 + k\gamma^2]dx \tag{5.2}$$

is valid where L is the length of the beam. The potential V of the loading is [Langhaar, 1962]

$$V = \frac{1}{2}\int_0^L Nv'^2 dx - \int_0^L qv dx - /_0^L Nu. \tag{5.3}$$

It is assumed that functions u^*, v^* and γ^* are such, that they minimize the potential energy Π. Let the functions u_0 and γ_0 be C^0 continuous and abritrary and let the function v^0 be C^1 continuous (function and its first dervative are continous) and arbitrary except that they satisfy the same boundary conditions as the functions u^*, v^* and γ^*. Let ε_0 be an arbitrary and small number and the following functions are substituted into the formula for the potential energy

$$u = u^* + \varepsilon_0 u_0, \tag{5.4}$$

$$v = v^* + \varepsilon_0 v_0, \tag{5.5}$$

$$\gamma = \gamma^* + \varepsilon_0 \gamma_0. \tag{5.6}$$

Thus the total potential energy Π is a function of the parameter ε_0 and a function of the functions u_0, v_0 and γ_0. According to the minimum principle for the potential energy the following equation is valid

$$\Pi(u, v, \gamma) \geq \Pi(u^*, v^*, \gamma^*). \tag{5.7}$$

By substitution the following equation can be derived

$$\Pi(u,v,\gamma) = \Pi(u^*,v^*,\gamma^*) = \varepsilon_0 \int_0^L [EAu^{*\prime}u_0' + B_0 v^{*\prime\prime}v_0'' + B_s(v^{*\prime\prime} - \gamma^{*\prime})(v_0'' - \gamma_0') + k\gamma^*\gamma_0 + Nv^{*\prime}v_0' - qv_0]dx - \varepsilon_0 /_0^L Nu_0 + \varepsilon_0^2 \left[U(u_0,v_0,\gamma_0) + \int_0^L Nv_0'^2 dx\right]. \quad (5.8)$$

It follows from the minimum principle (5.7) that

$$\varepsilon_0 B_1 + \varepsilon_0^2 B_2 \geq 0, for\ all\ \varepsilon_0, u_0, v_0, \gamma_0, \quad (5.9)$$

where the symbols B_1 and B_2 are found by comparing Eqs. (5.8) and (5.9). If the axial force N is zero or positive then it follows that $B_2 \geq 0$, for all u_0, v_0 and γ_0 because the strain energy is positive definite. Equation (5.9) is valid if for all u_0, v_0 and γ_0

$$B_1 = \int_0^L [EAu^{*\prime}u_0' + B_0 v^{*\prime\prime}v_0'' + B_s(v^{*\prime\prime} - \gamma^{*\prime})(v_0'' - \gamma_0') + k\gamma^*\gamma_0 + Nv^{*\prime}v_0' - qv_0]dx - /_0^L Nu_0 = 0. \quad (5.10)$$

On the other hand the axial force N always requires the additional condition for all u_0, v_0 and γ_0

$$B_2 = U(u_0,v_0,\gamma_0) + \int_0^L Nv_0'^2 dx \geq 0 => N \geq -\frac{U(u_0,v_0,\gamma_0)}{\int_0^L v_0'^2 dx}, \quad (5.11)$$

and the same result (5.10) results. Eq. (5.11) defines the stable constant (within elements of length L) axial force. By considering Eq. (5.10) the necessary conditions for the functions u, v and γ can be written in order that they minimize the potential energy.

Using the formulae for partial integration

$$\int_0^L fg'dx = /_0^L fg - \int_0^L f'gdx, \quad (5.12)$$

$$\int_0^L fg''dx = /_0^L fg' - /_0^L f'g + \int_0^L f''gdx, \quad (5.13)$$

it follows from Eq. (5.10) that

$$/_0^L(EAu' - N)u_0 + /_0^L(-B_0v''' - B_sv''' + B_s\gamma'' + Nv')v_0 + /_0^L(B_0v'' + B_sv'' - B_s\gamma')v_0' + /_0^L(-B_sv'' + B_s\gamma')\gamma_0 + \int_0^L EAu''u_0dx + \int_0^L(B_0v'''' + B_sv'''' - B_s\gamma''' - Nv'' - q)v_0dx + \int_0^L(B_sv''' - B_s\gamma'' + k\gamma)\gamma_0dx = 0. \quad (5.14)$$

Because the functions u_0, v_0, γ_0 and v_0' are abritrary except as regards the boundary conditions then the differential equations below follow from Eq. (5.14)

$$-EAu'' = 0, \tag{5.15}$$

$$Bv'''' - B_s\gamma''' - Nv'' - q = 0, \tag{5.16}$$

$$B_s v''' - B_s\gamma'' + k\gamma = 0, \tag{5.17}$$

and the boundary conditions

$$EAu' = N \vee u = 0 \ (\vee \ denotes \ or), \tag{5.18}$$

$$-Bv''' + B_s\gamma'' + Nv' = 0 \vee v = 0, \tag{5.19}$$

$$Bv'' - B_s\gamma' = 0 \vee v' = 0, \tag{5.20}$$

$$-B_s v'' + B_s\gamma' = 0 \vee \gamma = 0. \tag{5.21}$$

Consider first the differentail equations. Eq. (5.15) means that the axial force N is a constant, compare Eq. (1.12). From Eq. (5.17) it follows

$$-B_0 v''' + k\gamma - (B_0 v''' - B_s v''' + B_s\gamma') = 0 => \ M' = Q, \tag{5.22}$$

which is clearly the moment equilibrium equation of the differential free body of the beam. On the other hand from Eq. (5.17) follows with Eq. (5.18) that

$$B_s v''' - B_s\gamma'' = -k\gamma => B_0 v'''' - k\gamma' - Nv'' - q = 0 => Q' = -Nv'' - q, \tag{5.23}$$

which can be interpreted as theequilibrium equation of the lateral forces of the differential free body of the beam. By solving for the function γ from the equations

$$M = -Bv'' + B_s\gamma', \tag{5.24}$$

$$Q = -Bv''' + k\gamma, \tag{5.25}$$

and by using the equation $Q' = M''$ the following equation can be derived

$$v'''' - \frac{kB}{B_0 B_s} v'' = \frac{k}{B_0 B_s} M - \frac{M''}{B_0}. \tag{5.26}$$

This type of fundamental equation of the theory was derived by [Parland, 1946], [Granholm, 1949], [Pleskov, 1952], [Hoff & Mautner, 1948] and [Chitty, 1947] and it has been used widely for the analysis of many kinds of structures. This equation is suitable for the analysis of the shear walls, because they are often statically determined structures, cantilevers. Then the bending moment *M* can be calculated according to the equilibrium equations. The exact FEM has been derived, comprehensive computer programs written, based on Eq. (5.26) [Gluck, 1969], [Fransson, 1973].

A more general equation for the layered beam can be derived, if the following expression is substituted for the bending moment *M*

$$M = -Bv'' + B_s \left(\frac{Q'}{k} + \frac{B_0 v''''}{k} \right) = -Bv'' + B_s \left(-\frac{Nv''}{k} - \frac{q}{k} + \frac{B_0 v''''}{k} \right) \tag{5.27}$$

in Eq. (5.26) and then further manupulated. The result is

$$B_0 B_s v^{(6)} - (Bk + NB_s) v'''' + Nkv'' = B_s q'' - kq. \tag{5.28}$$

Substituting $q(x) = p(x) - cv(x) - \mu\omega^2 v(x)$ the final result is

$$B_0 B_s v^{(6)} - (Bk + NB_s) v'''' + (Nk + B_s c - B_s \mu\omega^2) v'' + (k\mu\omega^2 - kc) v = B_s p'' - kp. \tag{5.29}$$

The same equation without the term induced by the Winkler-type foundation has been derived for sandwich beams [Stamm & Witte, 1974].

The boundary conditions can be derived by considering Eqs.(5.18) – (5.21). Eq. (5.19) can be written as follows

$$-B_0 v''' + k\gamma + Nv' = 0 \vee v = 0 \Rightarrow Q + Nv' = 0 \vee v = 0. \tag{5.30}$$

Using the notation

$$Q_y = Q + Nv' \tag{5.31}$$

the homogeneous boundary condition is

$$Q_y = 0 \vee v = 0. \tag{5.32}$$

It follows from Eq. (5.20)

$$-M = 0 \vee v' = 0, \tag{5.33}$$

and from Eq. (5.21)

$$M_s = 0 \vee \gamma = 0. \tag{5.34}$$

The boundary conditions (5.31) – (5.33) can be written in the form

$$/_0^L\left(Q_y v - M v' + M_s \gamma\right) = 0. \tag{5.35}$$

Davies used these kinds of boundary conditions [Davies, 1986]. Eq. (5.35) can be transformed to the form

$$/_0^L\left(Q_y v - M v' + M_s \gamma\right) = /_0^L\left[Q_y v - M(v' - \gamma) + (M_s - M)\gamma\right] = /_0^L\left(Q_y v - M\varphi - M_0 \gamma\right) = 0, \tag{5.36}$$

and these are used in this study. As a motivation for this selection can be stated that the total rotation $\varphi = v' - \gamma$ is perhaps easier parameter to measure than the rotation v' used by Davies. Parland proposed [Parland, 1972] boundary conditions with the analogy between the bending of the layered beam and Vlasov's torsional theory.

The slip angle γ is needed in the boundary conditions and it can be derived from above and the result is

$$\gamma = -\frac{B_s}{k}\left[-\frac{B_0 v^{(5)}}{k} + \left(1 + \frac{N}{k}\right) v''' + \frac{(\mu\omega^2 - c)v'}{k} + \frac{p'}{k}\right]. \tag{5.37}$$

Figure 6 presents geometrical descriptions of the homogeneous buondary conditions.

$v = \varphi = \gamma = 0$ $v = \varphi = M_0 = 0$ $v = M = \gamma = 0$ $v = M = M_0 = 0$

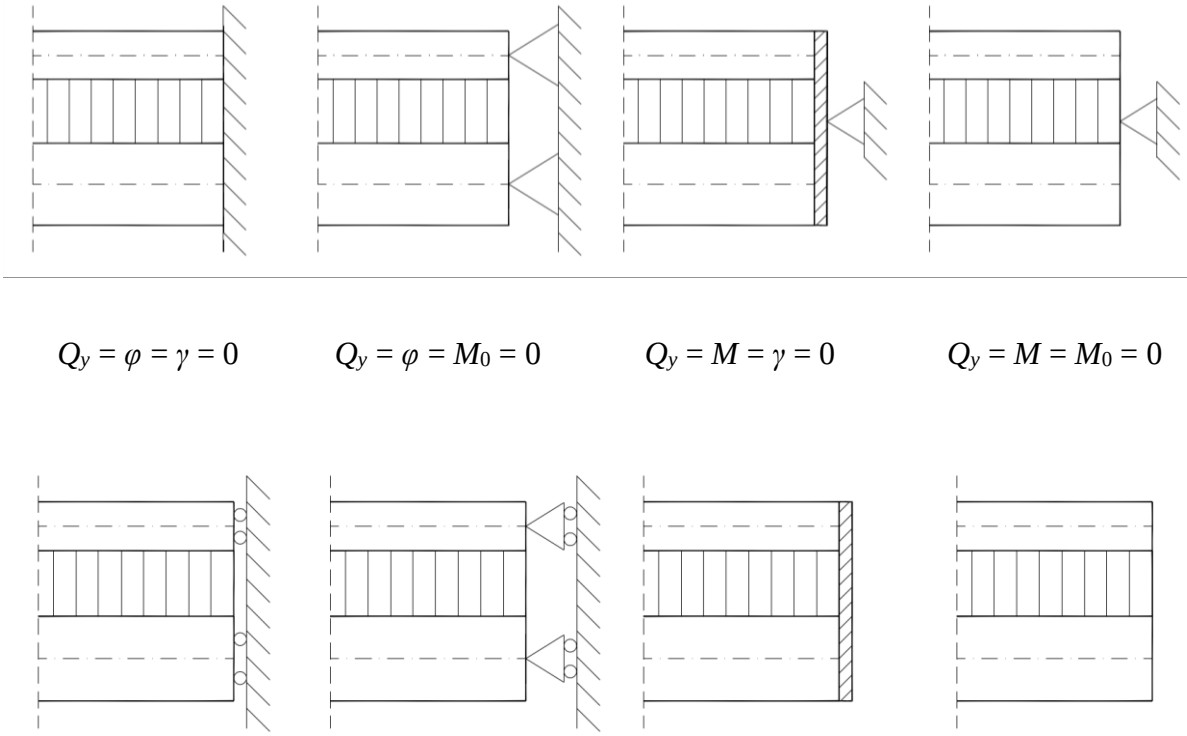

Figure 6. Homogeneous boundary conditions.

In the proposed theory, correponding displacements or stress resultants can be given at the ends of the beam and the complementary boundary conditions (5.35) are then

$$Q_y = \overline{Q_y} \vee v = \bar{v}, \tag{5.38}$$

$$M = \overline{M} \vee \varphi = \bar{\varphi}, \tag{5.39}$$

$$M_0 = \overline{M_0} \vee \gamma = \bar{\gamma}, \tag{5.40}$$

and the bar means the given value.

Solutions of the differential equation

Consider Eq. (5.28). It is a linear, sixth order differential equation and its solution can be written in the form

$$v = v_0 + v_1, \tag{6.1}$$

where the function v_0 is the general solution of the corresponding homogeneous differential equation and the function v_1 is some particular solution of the general equation (5.28). The general solution of the corresponding homogeneous differential equation is

$$v_0(x) = \sum_{t=1}^{6} C_{t,c} e^{r_t x}, \tag{6.2}$$

where parameters $C_{t,c}$ (t = 1, …, 6) are arbitrary complex numbers and r_t (t = 1, …, 6) are the roots of the characteristic equation. The characteristic equation will be a cubic equation [Heinisuo, 1989]. Its analytical solution was discovered by Scipione del Ferro ca. 1465-1526 [Boyer, 1968] and further improved by Cardan. The solution based on Lindelöf [Lindelöf, 1956] is given in Appendix A. Depending on the value of a discriminant D of the cubic equation, different solutions are obtained and many of those have been studied in [Heinisuo, 1989]. The particular solution v_1 depends on the loading of the beam. When the lateral load is uniform or trapezoidal, then the solution v_1 can be found easily. If there exists no lateral load then only the function v_0 is needed.

The equations $N = c = \mu = 0$ are valid in the case of bending of the layered beam. In this case $D = 0$. The solution v_0 is then

$$v_0(x) = C_1 \cosh \lambda x + C_2 \sinh \lambda x + C_3 + C_4 x + C_5 x^2 + C_6 x^3, \lambda = \sqrt{\frac{Bk}{B_0 B_s}}. \tag{6.3}$$

Two important special cases fall into the category $D < 0$, namely $c = \mu = 0$ (lateral bending + axial force) and $N = c = 0$ (tranverse vibration). The first of these cases has been studied in detail by Möttönen [Möttönen, 1987], while the second case has been studied in details by Malmi [Malmi, 1987], see also [Heinisuo et al, 1987] and [Heinisuo, 1988].

The exact FEM formulations using the solutions of the differential equations are given in [Heinisuo, 1989] and in [Davies, 2001] using different boundary conditions, see Eqs. (5.36) and (5.35). Other exact FEM formulations are such as [Monforton, 1979] and [Schwaze, 1984].

If the axial force is compressive and $c = \mu = 0$, and moreover the axial force satisfies the equation

$$-k\left(\frac{B_0}{B_s} + 1\right) < N < 0, \tag{6.4}$$

then the general solution v_0 is

$$v_0(x) = C_1 \cosh \lambda_1 x + C_2 \sinh \lambda_1 x + C_3 \cos \lambda_2 x + C_4 \sin \lambda_2 x + C_5 x + C_6, \tag{6.5}$$

where

$$\lambda_1 = \sqrt{\frac{1}{2}\left(-\frac{\alpha_2}{\alpha_1} + \sqrt{\frac{\alpha_2^2}{\alpha_1^2} - 4\frac{\alpha_3}{\alpha_1}}\right)}, \lambda_2 = \sqrt{\frac{1}{2}\left(\frac{\alpha_2}{\alpha_1} + \sqrt{\frac{\alpha_2^2}{\alpha_1^2} - 4\frac{\alpha_3}{\alpha_1}}\right)}, \tag{6.6}$$

$$\alpha_1 = B_0 B_s, \alpha_2 = -(Bk + NB_s), \alpha_3 = Nk. \tag{6.7}$$

The buckling load of the simply supported beam can be calculated by noting, that the function $v(x) = \sin(m\pi x/L)$ satisfies all the boundary conditions $v(0) = v(L) = M(0) = M(L) = M_0(0) = M_0(L) = 0$ meaning that the slips between the faces at the ends of the beam are free to occur. Substituting $v(x) = \sin(m\pi x/L)$ to the homogenous differential equations yields

$$B_0 B_s \frac{m^6\pi^6}{L^6} + (Bk + NB_s)\frac{m^4\pi^4}{L^4} + Nk\frac{m^2\pi^2}{L^2} = 0, \tag{6.8}$$

from which the critical compressive load can be solved

$$N_{cr} = \min\left(-\frac{B_0 B_s \frac{m^4\pi^4}{L^4} + Bk\frac{m^2\pi^2}{L^2}}{B_s\frac{m^2\pi^2}{L^2} + k}\right). \tag{6.9}$$

By varying the integer m in (6.9), the lowest value representing the buckling load N_{cr} can be found. Similarly the fundamental structural frequency f_0 of the simply supported beam based on the theory of layered beams [Stamm & Witte, 1974] is

$$f_0 = \frac{\omega_0}{2\pi} = \frac{1}{2\pi}\sqrt{\frac{B_s}{\mu L^4}\frac{1+\alpha+\alpha\beta m^2\pi^2}{1+\beta m^2\pi^2} m^4\pi^4}, \tag{6.10}$$

where

$$\alpha_i = \frac{B_i}{B_s}, \alpha = \sum_{i=1}^{n} \alpha_i = \frac{B_0}{B_s}, \tag{6.11}$$

$$\beta = \frac{B_s}{kL^2}. \tag{6.12}$$

Generally the solutions of the eigenvalue problems, critical loads, eigen frequencies, require the use of an algorithm originally developed by Williams and Wittrick [Williams & Wittrick, 1970] and further developed in [Howson & Williams, 1973]. It has been stated [Friberg, 1987] that the method of Williams and Wittrick in fact made possible the use of the exact finite element method when solving the eigenvalue problems.

If there exist e.g. tensile axial force and the Winkler-typed foundation then the case may fall to the category $D > 0$, but the sign of the discriminant is changing when the axial load is changing [Heinisuo, 1989].

Analytical solutions

Consider first bending ($N = c = \mu = 0$, $D = 0$) of the layered beam. The span of the beam is L and it is loaded with the uniform lateral load p, see Figure 7. The origin of the longitudinal axis is at the left end of the beam.

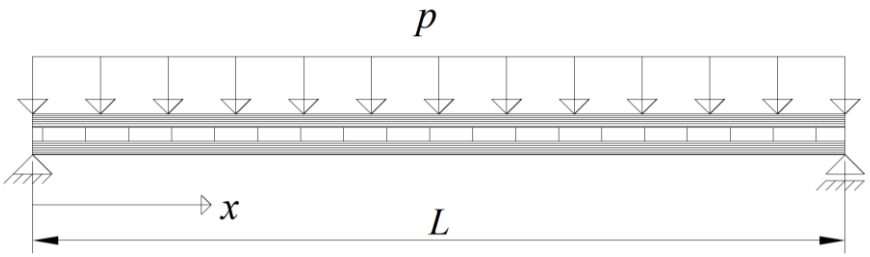

Figure 7. Simply supported beam with uniform lateral load.

Suppose that the faces are free to slip at both ends, then the boundary conditions are

$$v(0) = v(L) = M(0) = M(L) = M_0(0) = M_0(L) = 0. \tag{7.1}$$

The solution v_0 of the homogenious equation is shown in Eq. (6.3) and the particular solution is $v_1 = px^4/(24B)$. Using the dimensionless notation $\xi = x/L$ then the deflection $v(\xi)$ and the angle $\gamma(\xi)$ are [Stamm & Witte, 1974]

$$v(\xi) = \frac{pL^4}{B}\left[\frac{1}{24}\xi(1-2\xi^2+\xi^3) + \frac{1}{2\alpha\lambda^2}\xi(1-\xi) - \frac{1}{2\alpha\lambda^4}\frac{\cosh\left(\frac{\lambda}{2}\right)-\cosh\left(\frac{\lambda(1-2\xi)}{2}\right)}{\cosh\left(\frac{\lambda}{2}\right)}\right], \tag{7.2}$$

$$\gamma(\xi) = \frac{pL^3}{B}\beta\left[\frac{1}{2}(1-2\xi) - \frac{1}{\lambda}\frac{sinh\left(\frac{\lambda(1-2\xi)}{2}\right)}{cosh\left(\frac{\lambda}{2}\right)}\right]. \tag{7.3}$$

The stress resultants are

$$M(x) = \sum_{i=1}^{n} M_i + M_s = \frac{p}{L}(Lx - x^2), \tag{7.4}$$

$$M_s(\xi) = pL^2\frac{1}{1+\alpha}\left[\frac{1}{2}\xi(1-\xi) - \frac{1}{\lambda^2}\left(\frac{cosh\left(\frac{\lambda}{2}\right) - cosh\left(\frac{\lambda(1-2\xi)}{2}\right)}{cosh\left(\frac{\lambda}{2}\right)}\right)\right], \tag{7.5}$$

$$M_i(\xi) = pL^2\frac{\alpha_i}{1+\alpha}\left[\frac{1}{2}\xi(1-\xi) + \frac{1}{\alpha\lambda^2}\left(\frac{cosh\left(\frac{\lambda}{2}\right) - cosh\left(\frac{\lambda(1-2\xi)}{2}\right)}{cosh\left(\frac{\lambda}{2}\right)}\right)\right], \tag{7.6}$$

$$Q(x) = \sum_{i=1}^{n} Q_i + Q_s = \frac{p}{2}(L - 2x), \tag{7.7}$$

$$Q_s(\xi) = pL\frac{1}{1+\alpha}\left[\frac{1}{2}(1-2\xi) - \frac{1}{\lambda}\frac{sinh\left(\frac{\lambda(1-2\xi)}{2}\right)}{cosh\left(\frac{\lambda}{2}\right)}\right], \tag{7.8}$$

$$Q_i(\xi) = pL\frac{\alpha_i}{1+\alpha}\left[\frac{1}{2}(1-2\xi) + \frac{1}{\alpha\lambda}\frac{sinh\left(\frac{\lambda(1-2\xi)}{2}\right)}{cosh\left(\frac{\lambda}{2}\right)}\right]. \tag{7.9}$$

Suppose that the slips of the faces are prevented using some stiffeners at both ends, then the boundary conditions are

$$v(0) = v(L) = M(0) = M(L) = \gamma(0) = \gamma(L) = 0. \tag{7.10}$$

In this case the displacements and the stress resultants are

$$v(\xi) = \frac{pL^4}{B}\left[\frac{1}{24}\xi(1-2\xi^2+\xi^3) + \frac{1}{2\alpha\lambda^2}\xi(1-\xi) - \frac{1}{2\alpha\lambda^3}\frac{cosh\left(\frac{\lambda}{2}\right) - cosh\left(\frac{\lambda(1-2\xi)}{2}\right)}{sinh\left(\frac{\lambda}{2}\right)}\right], \tag{7.11}$$

$$\gamma(\xi) = \frac{pL^3}{B}\beta\left[\frac{1}{2}(1-2\xi) - \frac{sinh\left(\frac{\lambda(1-2\xi)}{2}\right)}{2\,sinh\left(\frac{\lambda}{2}\right)}\right], \tag{7.12}$$

$$M_s(\xi) = pL^2\frac{1}{1+\alpha}\left[\frac{1}{2}\xi(1-\xi) + \frac{1}{\lambda}\left(\frac{cosh\left(\frac{\lambda(1-2\xi)}{2}\right)}{2\,sinh\left(\frac{\lambda}{2}\right)} - \frac{1}{\lambda}\right)\right], \tag{7.13}$$

$$M_i(\xi) = pL^2 \frac{\alpha_i}{1+\alpha}\left[\frac{1}{2}\xi(1-\xi) - \frac{1}{\alpha\lambda}\left(\frac{cosh\left(\frac{\lambda(1-2\xi)}{2}\right)}{2\,sinh\left(\frac{\lambda}{2}\right)} - \frac{1}{\lambda}\right)\right], \tag{7.14}$$

$$Q_s(\xi) = pL \frac{1}{1+\alpha}\left[\frac{1}{2}(1-2\xi) - \frac{sinh\left(\frac{\lambda(1-2\xi)}{2}\right)}{2\,sinh\left(\frac{\lambda}{2}\right)}\right], \tag{7.15}$$

$$Q_i(\xi) = pL \frac{\alpha_i}{1+\alpha}\left[\frac{1}{2}(1-2\xi) + \frac{1}{\alpha}\frac{sinh\left(\frac{\lambda(1-2\xi)}{2}\right)}{2\,sinh\left(\frac{\lambda}{2}\right)}\right]. \tag{7.16}$$

Consider next bending of a simply supported one span beam, which is loaded by one concentrate load *F*. The span of the beam is *L*, see Figure 8. In this case no particular solution of the differential equation is needed.

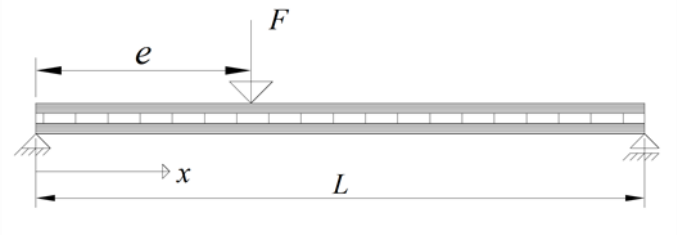

Figure 8. Simply supported beam with concentrated load.

The load is acting at $x = e$ and $\varepsilon = e/L$. At the simply supported supports the sliding is free to occur between timber and steel faces. The deflection of the beam is [Stamm & Witte, 1974]

$$v_1(\xi) = \frac{FL^3}{B}\left[\frac{1}{6}(1-\varepsilon)\xi(2\varepsilon - \varepsilon^2 - \xi^2) + \frac{1}{\alpha\lambda^2}(1-\varepsilon)\xi - \frac{1}{\alpha\lambda^3}\frac{sinh\lambda(1-\varepsilon)}{sinh\lambda}sinh\lambda\xi\right], \tag{7.17}$$

$$v_2(\xi) = \frac{FL^3}{B}\left[\frac{1}{6}\varepsilon(1-\xi)(-\varepsilon^2 + 2\xi - \xi^2) + \frac{1}{\alpha\lambda^2}\varepsilon(1-\xi) - \frac{1}{\alpha\lambda^3}\frac{sinh\lambda\varepsilon}{sinh\lambda}sinh\lambda(1-\xi)\right]. \tag{7.18}$$

where index 1 is valid for $0 \le \xi \le \varepsilon$ and index 2 is valid for $\varepsilon \le \xi \le 1$. The bending moments and shear forces are

$$M_{s1} = \frac{FL}{1+\alpha}\left[(1-\varepsilon)\xi - \frac{sinh\lambda(1-\varepsilon)}{\lambda sinh\lambda}sinh\lambda\xi\right], \tag{7.19}$$

$$M_{s2} = \frac{FL}{1+\alpha}\left[\varepsilon(1-\xi) - \frac{sinh\lambda\epsilon}{\lambda sinh\lambda}sinh\lambda(1-\xi)\right], \tag{7.20}$$

$$M_{i1} = \frac{FL\alpha_i}{1+\alpha}\left[(1-\varepsilon)\xi + \frac{sinh\lambda(1-\varepsilon)}{\alpha\lambda sinh\lambda} sinh\lambda\xi\right], \tag{7.21}$$

$$M_{i2} = \frac{FL\alpha_i}{1+\alpha}\left[\varepsilon(1-\xi) + \frac{sinh\lambda\varepsilon}{\alpha\lambda sinh\lambda} sinh\lambda(1-\xi)\right], \tag{7.22}$$

$$Q_{s1} = \frac{F}{1+\alpha}\left[1-\varepsilon - \frac{sinh\lambda(1-\varepsilon)}{sinh\lambda} cosh\lambda\xi\right], \tag{7.23}$$

$$Q_{s2} = \frac{F}{1+\alpha}\left[-\epsilon + \frac{sinh\lambda\varepsilon}{sinh\lambda} cosh\lambda(1-\xi)\right], \tag{7.24}$$

$$Q_{i1} = \frac{F\alpha_i}{1+\alpha}\left[1-\epsilon + \frac{sinh\lambda(1-\varepsilon)}{\alpha sinh\lambda} cosh\lambda\xi\right], \tag{7.25}$$

$$Q_{i2} = \frac{F\alpha_i}{1+\alpha}\left[-\epsilon - \frac{sinh\lambda\varepsilon}{\alpha sinh\lambda} cosh\lambda(1-\xi)\right], \tag{7.26}$$

where index 1 is valid for $0 \le \xi \le \varepsilon$ and index 2 is valid for $\varepsilon \le \xi \le 1$.

Consider the simply supported beam depicted in Figure 9. The sliding between the faces is prevented in the beam ends and the beam is loaded by an eccentric, with *e*, compressive axial forces -*N* at both ends. The boundary conditions are

$$a)\ v(\pm\tfrac{L}{2}) = 0\ , \qquad b)\ M(\pm\tfrac{L}{2}) = -e_0 N, \qquad c)\ \gamma(\pm\tfrac{L}{2}) = 0. \tag{7.27}$$

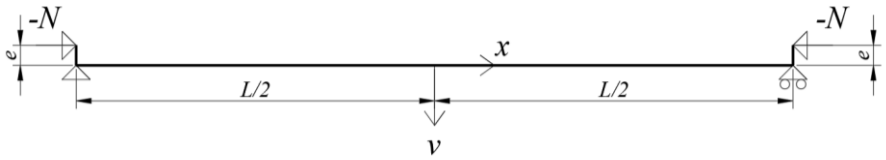

Figure 9. Layered beam loaded by eccentric axial loads at both ends.

Only the homogenious solution is needed and it is

$$v_0(x) = C_1 \cosh\lambda_1 x + C_2 \sinh\lambda_1 x + C_3 \cos\lambda_2 x + C_4 \sin\lambda_2 x + C_5 x + C_6, \tag{7.28}$$

in which the parameters C_i (i = 1,…, 6) are defined according to the boundary conditions (7.27). Assuming symmetric deflections with respect to the mid-span of the beam, then all the unsymmetric functions in (7.28) must vanish $C_2 = C_4 = C_5 = 0$. The first boundary condition implies

$$C_6 = -C_1 \cosh\frac{\lambda_1 L}{2} - C_3 \cos\frac{\lambda_2 L}{2}. \tag{7.28}$$

The third boundary condition implies

$$C_1 = \frac{\lambda_2^3 \sin\frac{\lambda_2 L}{2}\left(-\frac{B_0\lambda_2^2}{k}-1-\frac{N}{k}\right)}{\lambda_1^3 \sinh\frac{\lambda_1 L}{2}\left(-\frac{B_0\lambda_1^2}{k}+1+\frac{N}{k}\right)} C_3 = \frac{\alpha_4}{\alpha_5} C_3. \tag{7.29}$$

The second boundary condition implies in turn

$$C_3 = \frac{-e_0 N}{-B(\alpha_6-\alpha_7)+\frac{B_S^2 B_0}{k^2}\left(\lambda_1^4\alpha_6-\lambda_2^4\alpha_7\right)-\frac{B_S^2}{k}\left(1+\frac{N}{k}\right)\left(\lambda_1^2\alpha_6+\lambda_2^2\alpha_7\right)}. \tag{7.30}$$

The following parameters are used

$$\alpha_6 = \frac{\alpha_4}{\alpha_5}\lambda_1^2 \cosh\frac{\lambda_1 L}{2},\ \alpha_7 = \lambda_2^2 \cos\frac{\lambda_2 L}{2}. \tag{7.31}$$

If the presented beam problem boundary conditions are modified in a way, that the sliding between faces is free to occur at beam ends, we must replace the boundary condition $\gamma(L/2) = 0$ with a new condition $M_0\,(L/2) = 0$. In this case the homogenous solution parameter C_1 in (7.29) is replaced by

$$C_1 = \frac{\lambda_2^2 \cos\frac{\lambda_2 L}{2}}{\lambda_1^2 \cosh\frac{\lambda_1 L}{2}} C_3 = \frac{\alpha_4}{\alpha_5} C_3. \tag{7.32}$$

The equations for the parameters C_3 and C_6 remain unchanged. The stress resultants and the stresses are calculated as above.

Numerical examples

Bending of CLT beams

Consider cross-laminated timber (CLT) beams having 3-7 layers. In [Heinisuo & Pajunen, 2021] has been analyzed 24 cases using the theory of layered beams and the results are compared to test results, which are available in the referred literature. In the tests are reported the deflections at the elastic range and in some reports the measured strains are given. The number of identical tests varied being generally about 10. In the analyzed cases the cross-sections of the beams were symmetric. One case

with an unsymmetric cross-section was analyzed too and the results were compared to the FEM results. The cross-section of the CLT beam with five layers and the considered unsymmetric cross-section are presented in Figure 10. In the CLT beams the parallel direction layers, grains of the boards are parallel to the beam axis, act as the faces and the tranverse direction layers act as the cores.

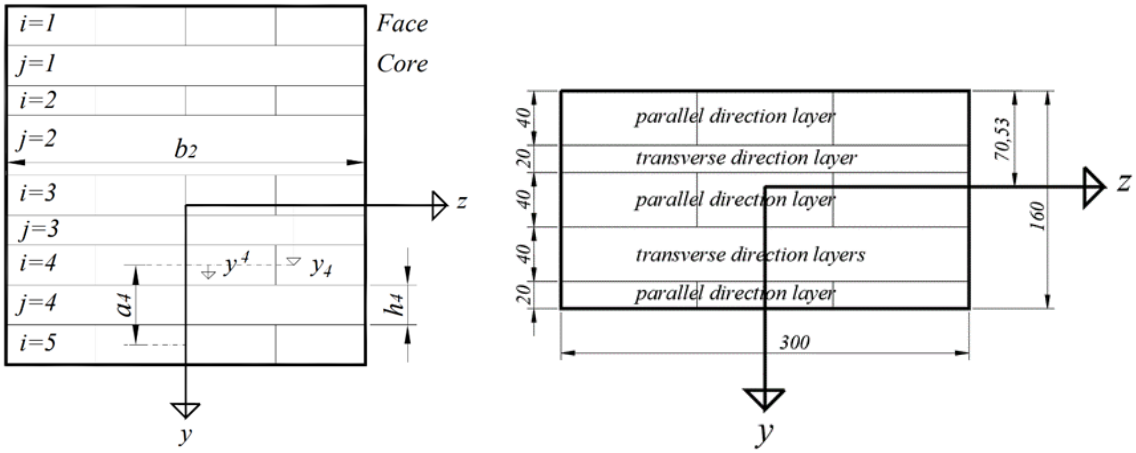

a) *b)*

Figure 10. Cross-sections of a) the 5-layer beam and b) unsymmetric beam.

Consider first four cases which are reported in [He et al, 2020]. Two long beams were loaded with the four point bending and two short beams were loaded with the three point bending. Widths of all beams were 310 mm. A dimension e is the distance from the support, see Figure 8. The measured Young's modulus of boards of the faces were E_i = 10925 MPa. The shear modulus of the faces (needed in the Timoshenko theory) were estimated using [EN 1995-1-1, 2014] as G_i = 10925/16 = 683 MPa and the shear modulus of the cores as 683/10 = 68.3 MPa. Other data and the results are given in Table 1.

The four point bending cases are analyzed by superposing two loading cases varying the distance e. These cases are analyzed also using the Timoshenko's theory and in this study using the theory of layered beams using the shear factor k proposed by Parland. The shear factor k of the beam with 3 layers (two faces and one core) are identical using the present shear factor Eq. (2.7) and Parland's shear facor Eq. (4.3). The beam with five layers (three faces and two cores) the error terms (4.8) are not same. In this case with five layers the shear factor of Parland is smaller than the present shear factor: $k_{\text{Parland}} = k_{\text{present}}/1.25$.

Table 1. Tested beams of [He et al, 2020].

Case	L (mm)	e (mm)	Densities (kg/m^3)	Layers (mm)	Total load (kN)	Measured deflection (mm)	Calculated deflection (mm)	Calculated deflection, Parland's shear factor (mm)	Deflection, Timoshenko's theory (mm)
Long 3 layers	3195	1282.5	490	35/35/35	13.49	26.7	30.0	30.0	27.8
Long 5 layers	4645	1857.5	486	35/25/35/25/35	14.80	34.6	34.9	35,4	32.6
Short 3 layers	575	287.5	490	35/35/35	30.00	1.2	1.2	30.0	1.8
Short 5 layers	845	422.5	486	35/25/35/25/35	60.00	2.2	2.4	2.8	3.6

It is seen, that the deflections using the theory are on the safe sides in all cases compared to the test results. The deflections using the Timoshenko theory not at the safe side in all cases. The deflections using Parland's shear factor are larger than measured deflections and the differences to the measured deflections are larger than using the present method, but the differences are not large.

The results of other tests results with the comparisions are shown in Table 2. The strains are calculated using Eq. (1.24) by multiplying the stress with the Young's modulus E_i.

Table 2. CLT beams.

Reference, case	Origin of modulus E_i	Total load (kN)	Measured deflection (mm)	Calculated deflection (mm)	Measured axial strain of bottom layer	Calculated axial strain of bottom layer
[Buka-Vaivade et al, 2017], 3-layers, span 1.8 m, four point bending	Handbook	5	7	8.7	0.0068	0.0067
[Buka-Vaivade et al, 2017], 3-layers, span 1.8 m, three point bending	Handbook	15	29	31.1	0.0028	0.0037
[Buck et al, 2016], 5-layers, span 1.71 m, four point bending	Handbook	60	16	18		
[Ceallaigh et al, 2018], 3-layers (20 mm), span 1.44 m, four point bending	Measured	20	14.5	15.8		

[Ceallaigh et al, 2018] 5-layers (20 mm), span 2.40 m, four point bending	Measured	20	16.7	18.5		
[Ceallaigh et al, 2018], 3-layers (40 mm), span 2.88 m, four point bending	Measured	20	14.6	15.8		
[Ceallaigh et al, 2018], 3-layers (20 mm), span 0.72 m, four point bending	Measured	40	-	3.9		
[Ceallaigh et al, 2018], 5-layers (20 mm), span 1.20 m, four point bending	Measured	40	-	2.2		
[Ceallaigh et al, 2018], 3-layers (40 mm), span 1.44 m, four point bending	Measured	40	4	3.9		
[Ruan et al, 2019], 3-layers, span 1.26 m, four point bending	Measured also G_j	20	3	3.1	0.00061	0.00057
[Ruan et al, 2019], 3-layers, span 1.89 m, four point bending	Measured also G_j	20	8	10.3	0.00106	0.00112
[Ruan et al, 2019], 3-layers, span 2.52 m, four point bending	Measured also G_j	20	21	23.8	0.00161	0.00167
[Christovasilis et al, 2016], 3-layers (19 mm), span 1.026 m, four point bending	Handbook	20	9.6	9.7		
[Christovasilis et al, 2016], 3-layers (19 mm), span 0.513 m, four point bending	Handbook	20	-	1.9		
[Christovasilis et al, 2016], 3-layers (44 mm), span 2.34 m, four point bending	Handbook	20	10.4	11.1		
[Christovasilis et al, 2016], 3-layers (44 mm), span 1.188 m, four point bending	Handbook	20	-	2.2		
[Christovasilis et al, 2016], 7-layers, span 5.4 m, four point bending	Handbook	20	9.9	11.0		
[Christovasilis et al, 2016], 7-layers, span 2.7 m, four point bending	Handbook	20	-	2.4		
[Zhang et al, 2017], 5-layers, span 3.15 m, four point bending	Handbook	20	9.0	9.7		
[Zhang et al, 2017], 5-layers, span 3.15 m, four point bending, rotated 90^o from pervious	Handbook	10	16.6	19.5		

It is seen that the calculated deflections are in almost all cases larger than measured deflections and the theory of the layered beams simulates well the deflections and axial strains in the considered cases.

Consider next the unsymmetric beam of Figure 10 b). This case introduces the structure, where the Generalized Bernoulli's hypothesis is not presumably valid. The cross-section is composed of three faces and the shear factor is defined considering two layers in the transverse direction. The elastic properties of the grade C24 are as they are given in [Borgström & Fröbel, 2019]: parallel direction E_i = 11000 MPa, transverse direction G_j = 50 MPa. A simply supported beam of the span 3 m is considered with a concentrated load 15 kN located at 1 m from the left support, see Figure 8. In the FEM simulations the shear modulus of the parallel layer was G_i = 690 MPa and the Young's modulus of the transverse layer was E_j = 370 MPa, and the Poisson' ratio was 0.3 both in the parallel direction and in the transverse direction.

Comparisons of the results of the layered beam theory were done in [Heinisuo, Pajunen, 2021] with the results of the FE-models using a program Autodesk Robot Structural Analysis Professional, Version 33.0.6930 (x64). Square four node plane stress elements with an orthotropic material were used. The FEM model was validated with the tests of [Ruan et al, 2019]. The used element sizes were 5 mm x 5 mm and 2.5 mm x 2.5 mm.

The maximum deflection using the theory of layered beams was 10.7 mm and using the FEM 9.6 mm. In this case $k_{\text{Parland}} = k_{\text{present}}/0.84$ and the deflection using Parland's shear factor is 10.4 mm. In [Heinisuo, Pajunen, 2021] is calculated the deflection applying the theory of the layered beams for this beam with five faces, considering the transverse layers as the faces, too. The deflection was then 10.6 mm. The axial stresses at the loading point are given in Figure 11.

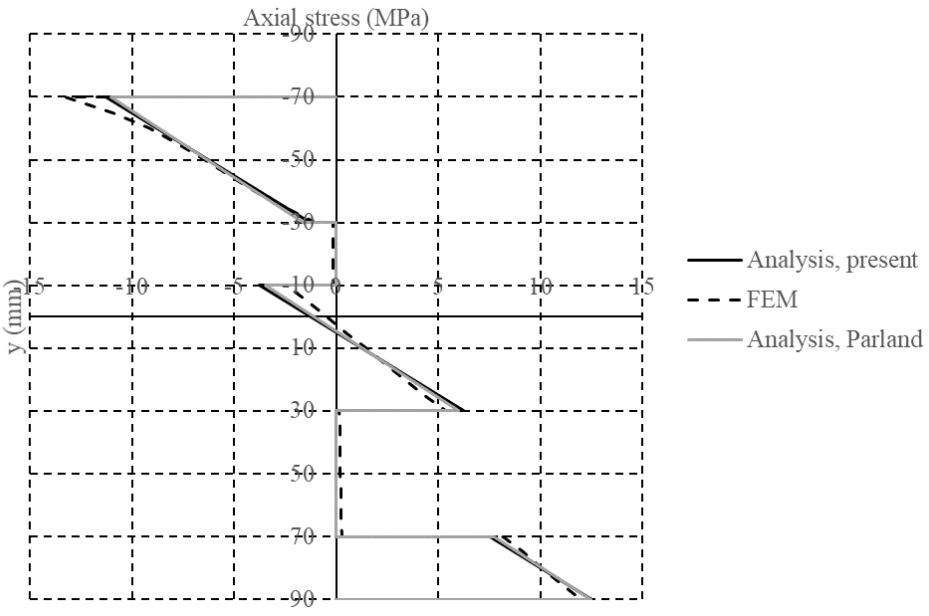

Figure 11. Axial stresses at load point of unsymmetric beam. FEM result with goarser mesh.

In Figure 11 can be seen, that the axial stresses at the lower part of the cross-section fit rather well using the theory of layered beams to the FEM results, the maximum tensile stresses being 12.6 MPa and 12.0, respectively. Using the FEM, the stresses of the top surface are larger due to the stress concentration near the loading point and the resuls did not change with the finer mesh. The deflection using Parland's shear factor is nearer the FEM results than using the present theory.

A refined mesh (FEM_2) using the element size of 2.5 mm x 2.5 mm was used, too. The concentrated load was given as 9 nodal loads distributed to 20 mm. Displacements and axial stresses did not change compared the results using the element size of 5 mm x 5 mm. The shear stresses of the FEM are taken 10 mm from the theoretical point load, i.e. at the section where the last nodal force is acting. The shear stresses are shown in Figure 12.

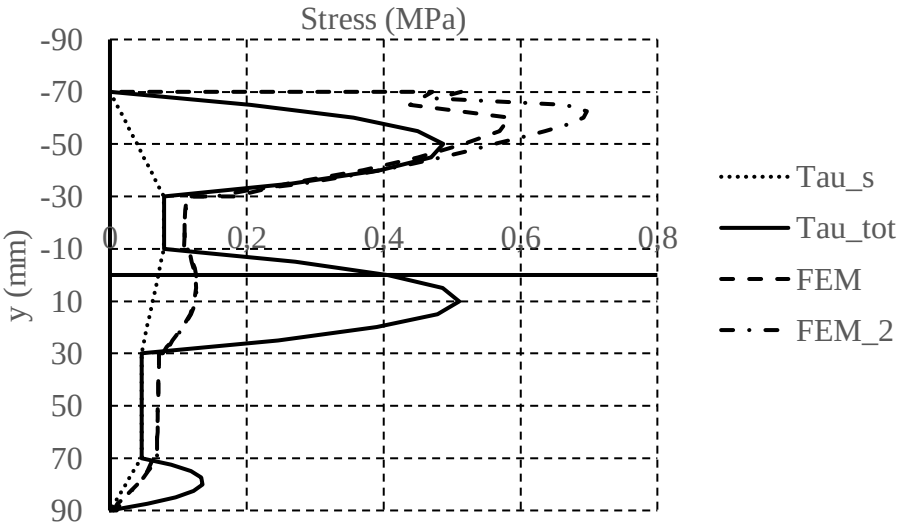

Figure 12. Shear stresses at load point of unsymmetric beam at the loading point, left side.

The mesh size had a considerable effect to the shear stresses near the top surface, as can be seen in Figure 12, FEM_2. The shear stresses of other layers did not change when changing from FEM to FEM_2. The shear stresses in the transverse direction are near FEM results using the theory of layered beams, but the shear stresses of two lowest parallel layers are larger than FEM results.

Bending and vibration of steel-timber composite beams

Consider next the steel-timber composite beams. In [Hassanieh et al, 2017] are given the results of 7 tests. In this study are considered four of these tests. In these cases the CLT-slabs were connected above the steel beams using different connection techniques and varying the steel profiles and the orientation of the CLT-slabs. The starts of the yield of the steel beams and the corresponding deflections were reported in the tests, together with load-deflection diagrams and ultimate loads. In [Hassanieh et al, 2016] are given the results of 7 tests where LVL-slabs were connected above the steel beams using different connection techniques and varying the steel profiles. Unfortunately, the starts of the yields and the corresponding deflections were not reported so they are not considered here. In [Chiniforush et al, 2019] are presented the experimental and 3D FEM results of impact hammer tests with six different steel-composite beams. Two of them, S1CS$\big|\big|$ and S2DS$\big|\big|$ are considered here using the theory of the layered beams. C refers to the connection of two 16 mm coach screws with l_s = 250 mm and D refers to two 16 mm dog screws with l_s = 250 mm. Vertical bars refers to the top layers of CLT, which are parallel to the beam axis.

The steel-CLT composite beam tests were completed using the four point bending. These beams were analyzed superposing two point loaded beams according to Figure 8. The cross-sections of the beams were modelled as a layered beam with two faces: the CLT-slab and the steel profile. The connections between those, the cores, are constructed of the pairs of mechanical connectors between the CLT-slabs and the steel profiles. The Young's modulus of the CLT slab was defined as a EA-equivalent modulus based on the measured Young's modules 12000 MPa in the grain direction and given [Hassanieh et al, 2019] elastic modulus of C24 spruce layers in the perpendicular grain direction 730 MPa. In [Aspila et al, 2022] are calculated the same cases using the EI-equivalent modules for the CLT. The data which is used in the theory of the layered beams of the Case 1 is given in Table 3.

Table 3. Data of Case 1 of [Hassanieh et al, 2017].

CLT outer layer orientation with respect to beam	Parallel
Span L (mm)	5850
Loading points ε	0.329, 0.671
Layers of CLT (mm)	20/20/40/20/20
E_1 (MPa)	8243
Measured density of CLT (kg/m^3)	490
Steel profile	310UB32.0
Measured yield strength of steel profile (MPa)	350
Given Young's modulus of steel profile E_2 (MPa)	200000

Connection type for steel-CLT joint	Two 16 mm coach screws
Length of screws (mm)	100
Connection spacing l_s (mm)	250
Measured [Hassanieh et al, 2017b] mean slip moduli $k_{s,0.4}$ of two coach screws for steel-CLT joint (kN/mm). In this study $k_s = k_{s,0.4}$	22.23

In Figure 13 are presented the deflections v1 and v2 for the point loads 95 kN and their sum for the total load 190 kN in the Case 1.

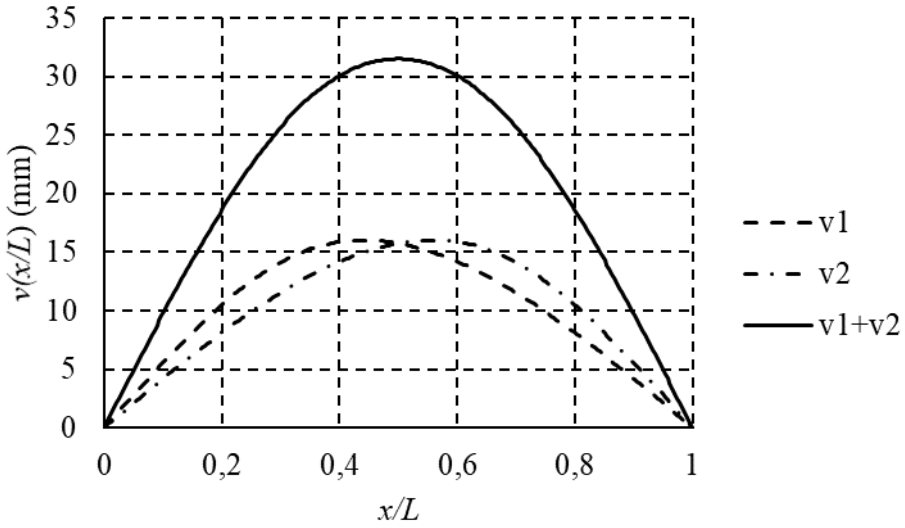

Figure 13. Deflections of the Case 1.

In Figures 14 and 15 are shown the bending moments and the shear forces of the Case 1.

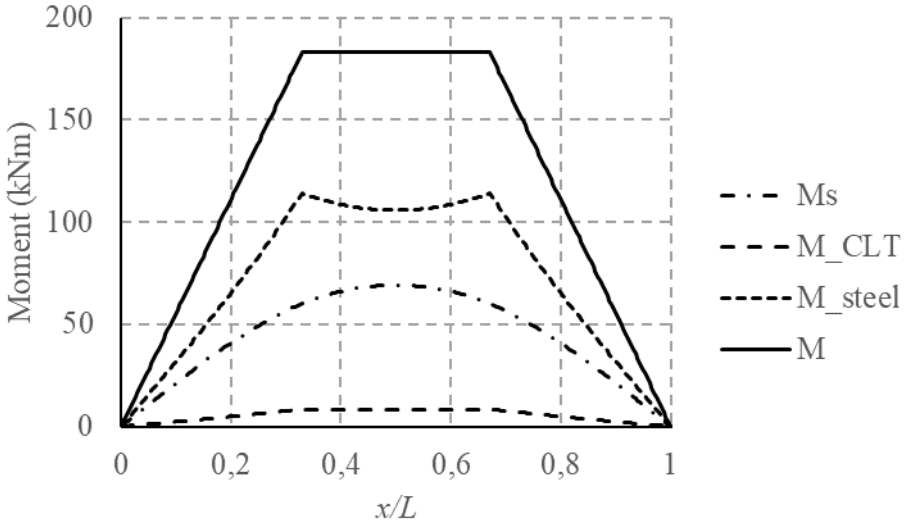

Figure 14. Bending moments of the Case 1.

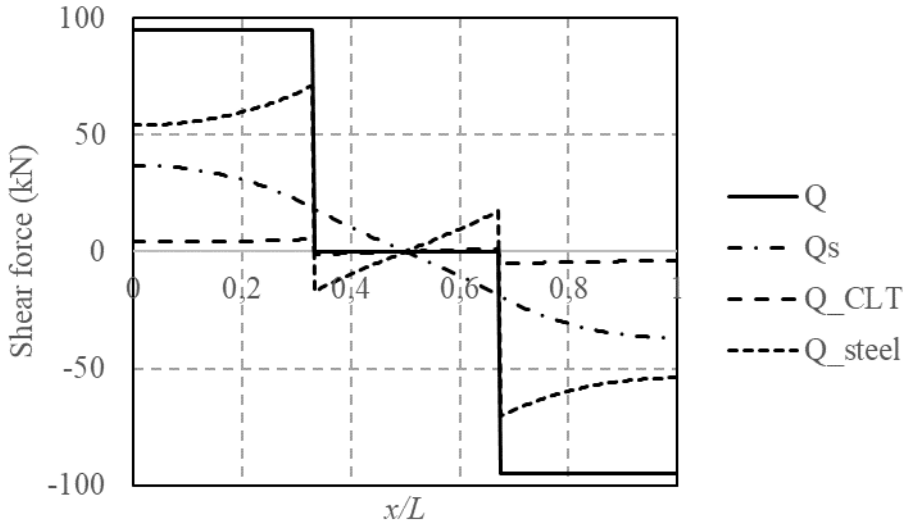

Figure 15. Shear forces of the Case 1.

It is seen that the steel beam carries the main part of the load. The shear force is Q_s = 36.9 kN at the end of the beam and from this follows the force of the connection using Eq. (3.2) $Q_s l_s/a_1$ = 39.1x250/209 = 44.2 kN.

The Case 2 is like the Case 1, but the connections between steel and timber were completed using 2M16 (8.8) bolts and the steel beam 310UB40.4. Based on experiments in [Hassanieh et al, 2016] is given a seven-parameter model to calculate the force-slip relation for this and for many other connections. Using this model, the shear stiffness is k_s = 15.03 kN/mm.

The Case 3 is like the Case 1, but the connection between timber and steel is completed with two dog screws with 19 mm diameters, spacings 300 mm and lengths 135 mm. The stiffness of the connection is k_s = 17.16 kN/mm.

In the Case 4 the CLT slabs are rotated 90 degrees with respect to the previous cases. Using the EA-equivalent elastic modulus for CLT the result is E_1 = 4487 MPa. The steel beam was 250UB25.7. The connections were completed using two coach screws with the shear stiffness k_s = 6.81 kN/mm.

The results of the Cases 1-4 are given in Table 4.

Table 4. Results of Cases 1-4.

Case		Analysis	Test
1	Yield load (kN)	190	208
	Maximum deflection at yield (mm)	31.5	31.8
	Peak load (kN)		267
2	Yield load (kN)	241	251
	Maximum deflection at yield (mm)	33.4	30.9
	Peak load (kN)		336
3	Yield load (kN)	185	214
	Maximum deflection at yield (mm)	33.6	32.3
	Peak load (kN)		287
4	Yield load (kN)	179	202
	Maximum deflection at yield (mm)	20.7	21.2
	Peak load (kN)		270

The test beams in the vibration tests had spans 5.8 m. The width of the CLT-slab was 1000 mm and the thickness 120 mm. The shear stiffness of two coach screws is, see Case 1, k_s = 22.23 kN/mm. The shear stiffness of two dog screws is [Hassanieh et al, 2017b] k_s = 29.65 kN/mm. The elastic modulus of CLT is E_i = 8243 MPa and the steel profile is 310UB32.0, see Case 1.

In [Chiniforush et al, 2019] are given many analytical formulae for prediction of the fundamental frequency of the first bending mode. Many of these are based on the bending stiffness of the beam. In [Chiniforush et al, 2019], for the comparisons with the tests and with the advanced FEM calculations, the bending stiffness is calculated back from the tests results, as in [Loss & Davison 2017]. In Table 5 are presented the results for two cases. The fundamental structural frequencies are calculated using Eq. (6.10).

Table 5. Fundamental structural frequencies [Hz] of steel-timber composite beams.

Case	Present study	Test	FEM	Wyatt [1]	Wyatt [2]	Murray	Allen	Eurocode 5
S1CS	22.75	24.16	23.80	22.02	21.71	21.72	19.28	21.72
S2DS	23.48	24.65	23.80	22.75	22.43	22.44	19.92	22.44

It is seen that the theory of layered beams simulates rather well the test results of steel-CLT composite beams in the considered cases.

Bending and axially loaded CLT beams

A total of 12 five-layer CLT beams were tested under concentric and eccentric axial loads in [Huang et al, 2022]. The eccentricity of the axial load means bending of the beam out-of-plane. In [Sultan & Di Leonardo, 2015] has been reported 8 tests under eccentric axial loads varying the number of layers

and eccentricities. These tests are analyzed here using the elastic theory of the layered beams. In the tests were observed that the ultimate failure modes of such structures are compression crush on the concave side or tension rupture on the convex side, while the rolling shear stress in transverse layers is elastic up to the failure. This observation enables the estimation of the failure load using the elastic theory when the stress limits are defined both for the compression and tension side. In this study the stress limits are defined as 0.8 times the measured compression and tension streghts in the grain direction of the outmost layers. The axial stresses are calculated using Eq. (1.24).

In [Huang et al, 2022] 12 tests using pairs of identical specimen were completed. The data of the tests is presented in Table 6.

Table 6. Material properties and tested beam dimension according to [Huang et al, 2022]

$h_i = h_j$ (mm)	h (mm)	b (mm)	L (mm)	E_i (MPa)	Tensile elastic limit (MPa)	Compression elastic limit (MPa)	Rolling shear strength (MPa)	G_j (MPa)
35	175	200	3600	11465	0.8*37	0.8*46	1.12	336

The tests were completed with zero eccentricity and varying the eccentricities up to the height h of the beam. In [Huang et al, 2022] is given an analytical formule for the estimation of the ultimate load. In Table 7 are given the results. The ultimate load with zero eccentrity is calculated using the buckling load of Eq. (6.9) and the cases with the eccentricities are calculated based on the solution in Eq. (7.28), see Figure 9. It is written in [Huang et al, 2022] that the boundary conditions at the ends of the beams were such that the slips are free to occur between the faces. In the tests, the CLT ends were connected to steel brackets with four 19 mm bolts, which may support the boundary conditions with no slips. The calculation were done using these boundary conditions.

Table 7. Results of five-layer beams.

Eccentricity (mm)	N_u (kN) mean of two tests	N_u (kN), analytical formula [Huang et al, 2022]	Difference to the tests (%)	N_u (kN), proposed method	Difference to the tests (%)
0	540.5	-	-	599	10.82
$h/6 = 29.17$	311	311	0	292.76	-5.86
$h/3 = 58.33$	216.5	196	-9.47	217.05	0.25
$h/2 = 87.50$	192	152	-20.82	175.20	-8.75
$3h/4 = 131.25$	142	122	-14.08	137.17	-3.40
$h = 175.00$	110	107	-2.73	113.24	2.95

The results are shown in Figure 16.

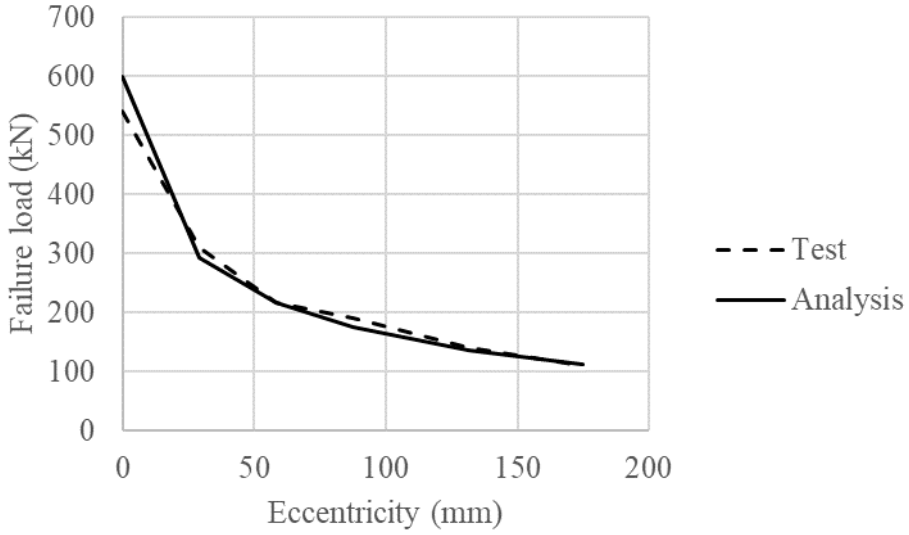

Figure 16. Ultimate loads of five-layer beams.

The calculated axial stresses are given in Table 8.

Table 8. Axial stresses at the mid-span, five-layer beam.

Eccentricity (mm)	N_u (kN), proposed method	Compressive stresses (MPa)	Tensile stresses (MPa)
0	599	28.50	-
$h/6 = 29.17$	292.76	36.80	8.92
$h/3 = 58.33$	217.05	36.80	16.12
$h/2 = 87.50$	175.20	36.80	20.11
$3h/4 = 131.25$	131.17	36.80	23.73
$h = 175.00$	99.05	36.80	26.02

It is seen that the compression sides were critical in all cases. The same cases were calculated also using the boundary conditions allowing slips of the faces at the ends of the beam. The shear stresses of the transverse layers are shown in Figure 17 near the end of the beam.

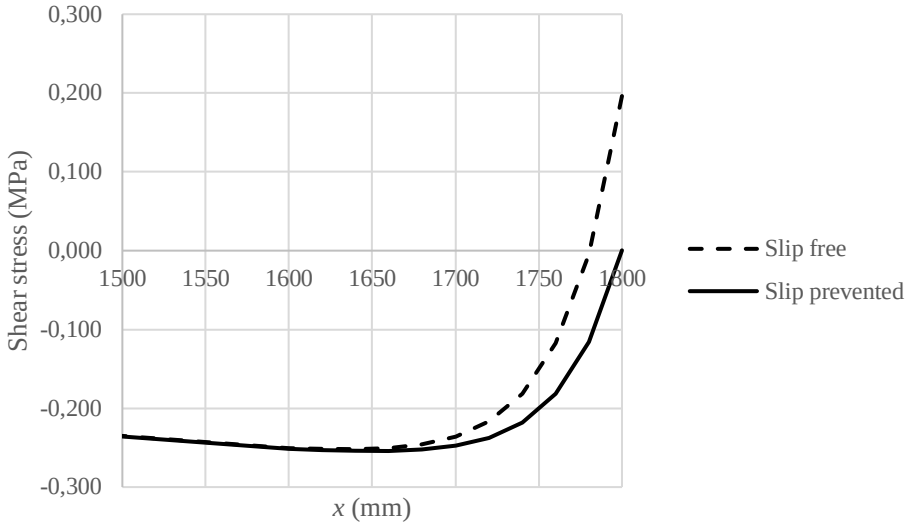

Figure 17. Shear stresses of transverse layers, five-layer beam.

In figure 17 can be seen the stress concentrations of the shear stresses near the supports. The shear stresses are not close to the respective strength values. It should also be noted that the shear stress distribution of the transverse layers is quite different to the one presented in [Huang et al, 2022].

The material data of 8 tests in [Sultan & Di Leonardo, 2015] were same as above. The test data and results are shown in Table 9.

Table 9. Test data and results of [Sultan & Di Leonardo, 2015].

Test	Number of layers	$h_i = h_j$ (mm)	h (mm)	b (mm)	L (mm)	e_0 (mm)	N_u tests (kN)
E1-T1	7	34.43	241	600	3600	1.5	3118
E1-T2	3	33.33	100	600	3600	3.0	1046
E1-T3	7	34.43	241	600	3600	84.0	1044
E1-T4	3	33.33	100	600	3600	40.0	240
E1-T5	7	34.43	241	600	3600	41.5	1447
E1-T6	3	33.33	100	600	3600	21.5	310
E1-T7	3	33.33	100	600	3600	18.0	320
E1-T8	3	33.33	100	600	3600	62.0	240

Comparisons between results based on tests, proposed method, and analytical formula derived in [Huang et al, 2022] are given in Table 10.

Table 10. Comparisions of results.

Test	N_u test (kN)	N_u (kN), analytical formula of [Huang et al, 2022]	Difference to the tests %	N_u (kN) present theory	Difference to the tests %
E1-T1	3118	-	-	2759	-11.51
E1-T2	1046	-	-	384	-63.29
E1-T3	1044	867	-16.95	933	-10.63
E1-T4	240	298	24.17	226	-5.83
E1-T5	1447	1273	-12.02	1325	-8.43
E1-T6	310	482	55.48	280	-9.68
E1-T7	320	548	71.25	294	-8.13
E1-T8	240	211	-12.08	186	-22.50

The present theory is on the safe side in all cases, whereas the analytical formula of [Huang et al, 2022] estimates the ultimate loads with bigger errors and gives highly unsafe estimations in two cases. In the case E1-T2 the experimental test result for ultimate failure load is 1046 kN, which is essentially higher, than the elastic buckling load. Using the layered beam theory, the buckling load value is 415 kN, and using the proposed method with stress constraints, the ultimate failure load value of 384 kN is obtained.

Temperature and moisture loadings

Consider the case where temperature or moisture loadings are acting to the beam. The beam with two faces are considerd. Figure 18 shows the temprature T_{ik} or moisture P_{ik} distributions of the faces. Here k refers to top $k = 1$ or bottom $k = 2$ egde of the face i. It is supposed that the distributions are linearly distributed to the faces.

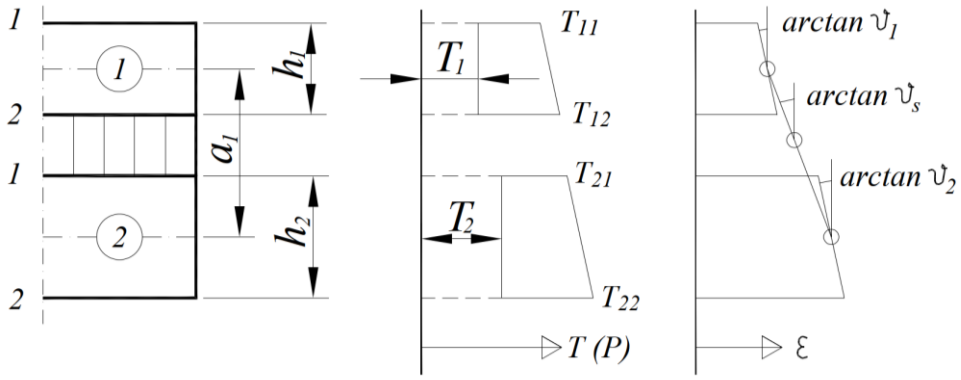

Figure 18. Temperature and moisture distributions and strains.

The longitudinal strains of the faces due to these displacement actions can be represented by the equations, referring to Figure 18

$$\varepsilon_{ik} = \alpha_{T_i}(T_{ik} - T_i), i = 1,2; k = 1,2, \tag{8.1}$$

or

$$\varepsilon_{ik} = \alpha_{P_i}(P_{ik} - P_i), i = 1,2;\ k = 1,2, \tag{8.2}$$

where α_{Ti} (i = 1, 2) are the coefficients of thermal expansion of the faces (dimension per degree Cesius), α_{Pi} are the coefficients of moisture expansion of the faces (dimension per percent), and T_i and P_i are the initial temperature and moisture contents of the faces, assumed as contants at the faces. The loading ε_{ik} causes elongations of the beam-axis x and this effect is not considered in this study. These loadings also cause changes in curvature of the beam. The parameter ϑ_s is the curvature measured at the centroids of the faces and the parameters ϑ_i (i = 1, 2) are the curvatures of the faces so that

$$\vartheta_s = \frac{(\varepsilon_{22}+\varepsilon_{21})-(\varepsilon_{12}+\varepsilon_{11})}{2a_1}, \tag{8.3}$$

$$\vartheta_i = \frac{\varepsilon_{i2}-\varepsilon_{i1}}{h_i}, i = 1,2. \tag{8.4}$$

The bending moments are

$$M_0 = -B_0(v'' + \vartheta_1 + \vartheta_2), \tag{8.5}$$

$$M_s = -B_s(v'' - \gamma' + \vartheta_s), \tag{8.6}$$

$$M = -Bv'' + B_s\gamma' - B\vartheta, \tag{8.7}$$

where

$$\vartheta = \frac{B_s}{B}\vartheta_s + \frac{B_1}{B}\vartheta_1 + \frac{B_2}{B}\vartheta_2, \tag{8.8}$$

and the loading term $Bk\vartheta$" has to be added to the differential equation (5.29), and other equations of the theory hold.

The case where $\vartheta_1 = \vartheta_2 = 0$ has been studied in [Stamm & Witte, 1974] and the work equivalent nodal forces for the exact finite element formulations have been derived in [Davies, 1986] and in [Möttönen, 1987], if the displacement loading is assumed to be a constant within the element. The more general case presented above has been studied in [Aicher & Noack, 1987]. They used the analytic solution of the differential equation, and also using the approximative FEM, where the faces are modelled by the Bernoulli-Euler beam elements and the core is modelled by rectangular plane elements (eight nodes/element). They studied the one-span beam made of plywood faces connected with a polyurethane core and loaded by a moisture loading. The authors concluded that in order to get accurate results the element mesh must be refined near the supports of the beam, and 17 plane elements and 68 beam elements had to used for one half of the simply supported beam. In [Heinisuo, 1989] was shown that the use of one element based on the exact FEM for the half of the beam gives accurate results for design purposes. Steel-polyurethane-steel sandwich beams with 1-3 spans loaded by temperature loadings have been studied in [Chong et al, 1977], [Stamm, 1984], [Davies, 1985], [Möttönen, 1987], [Heinisuo, 1987], [Heinisuo et al, 1987].

Consider the one-span (L = 2500 mm) beam as in [Aicher & Noack, 1987] and in [Heinisuo, 1989]. The beam is made of plywood faces connected with a polyurethane core and loaded by a moisture loading. The cross-section and the moisture loadings are shown in Figure 19.

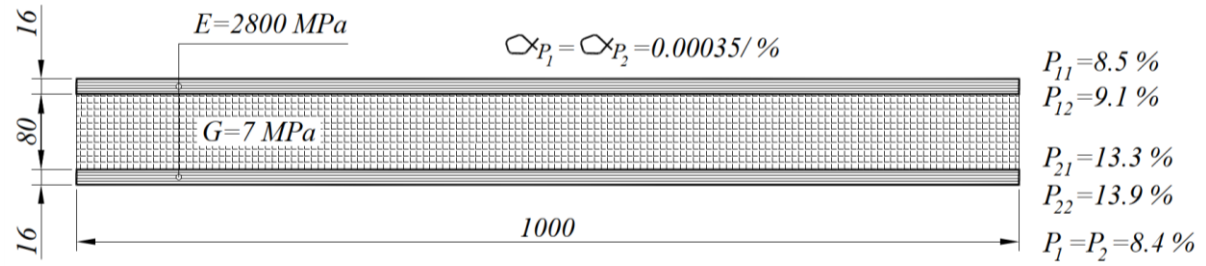

Figure 19. Cross-section of the beam with moisture loadings.

In [Aicher & Noack, 1987] and [Heinisuo, 1989] the beam was simply supported at both ends. In this study eight boundary conditions are given at both ends of the beam, as is illustrated in Figure 6. The displacement loading is assumed to be a constant along the beam and the equations $N = c = \mu = 0$ are valid. The origin of longitudinal x axis is located at the mid-span of the beam and the deflection function is symmetric. The deflection v(x) of the beam is

$$v(x) = C_1 \cosh \lambda x + C_2 + C_3 x^2, \lambda = \sqrt{\frac{Bk}{B_0 B_s}}, \tag{8.9}$$

where the parameters C_i (i = 1, 2, 3) are defined using the boundary conditions. The quantities which are needed in the calculations are

$$\varphi(x) = v^{(1)}(x) - \gamma(x) = -\frac{\lambda B_0}{B_s} C_1 \sinh \lambda x + 2C_3 x, \tag{8.10}$$

$$\gamma(x) = -\frac{B_s}{k}\left(-\frac{B_0}{k} v^{(5)} + v^{(3)}\right) = \frac{\lambda B}{B_s} C_1 \sinh \lambda x, \tag{8.11}$$

$$Q = -B_0 v^{(3)} + k\gamma = 0, \tag{8.12}$$

and see Eqs. (8.5), (8.7)

$$M = -2BC_3 - B\vartheta, \tag{8.13}$$

$$M_0 = -B_0 \lambda^2 C_1 \cosh \lambda x - 2B_0 C_3 - B_0(\vartheta_1 + \vartheta_2), \tag{8.14}$$

The initial data is shown in Table 11.

Table 11. Initial data of example.

L (mm)	2500
a_1 (mm)	96
$h_1 = h_2$ (mm)	16
ε_{11}	3,50E-05
ε_{12}	2,45E-04
ε_{21}	1,72E-03
ε_{22}	1,93E-03
ϑ_s (1/mm)	1,75E-05
$\vartheta_1 = \vartheta_2$ (1/mm)	1.31E-05
ϑ (1/mm)	1.75E-05
B_s (Nmm^2)	2.06E+11
B_1=B_2 (N/mm^2)	9.56E+08
B (N/mm^2)	2,08E+11
k (N)	806400
λ (1/mm)	0.0206

Use of fixed supports numbered as 1 in Figure 6 at both ends with the boundary conditions $v = \varphi = \gamma = 0$, then the parameters $C_i = 0$ for all i = 1, 2, 3. Note, that the elongation of the beam axis and the

corresponding axial force are not condered. Other quantities but the moments disappear. Based on Eqs. (8.13) and (8.14) the uniform moments are

$$M = -B\vartheta = -3.638\ kNm, M_1 = M_2 = -0.025\ kNm, M_s = M - M_0 = -3.588\ kNm. \quad (8.15)$$

The moments M_i cause the bending stresses +/- 0.59 MPa to the faces and the moment M_s causes the axial stesses +/- 2.34 MPa to the faces.

The boundary conditions number 2 in Figure 6 at both ends lead to the following parameters

$$v(L/2) = 0 => C_1 \cosh \lambda L/2 + C_2 + C_3(L/2)^2 = 0 => C_2 = -C_1 \cosh\frac{\lambda L}{2} - C_3\left(\frac{L}{2}\right)^2, \quad (8.16)$$

$$\varphi(L/2) = 0 => -\frac{\lambda B_0}{B_s} C_1 \sinh\frac{\lambda L}{2} + 2C_3\left(\frac{L}{2}\right) = 0 => C_3 = \frac{\lambda B_0}{LB_s} C_1 \sinh\frac{\lambda L}{2}, \quad (8.17)$$

$$M_0(L/2) = 0 => -B_0\lambda^2 C_1 \cosh\frac{\lambda L}{2} - 2B_0C_3 - B_0(\vartheta_1 + \vartheta_2) = 0 => C_1 = \frac{-(\vartheta_1+\vartheta_2)}{\lambda^2\left(\cosh\frac{\lambda L}{2} + \frac{2B_0}{B_S\lambda L}\sinh\frac{\lambda L}{2}\right)}. \quad (8.18)$$

The deflections, shear forces and the moments are shown in Figures 20 – 23.

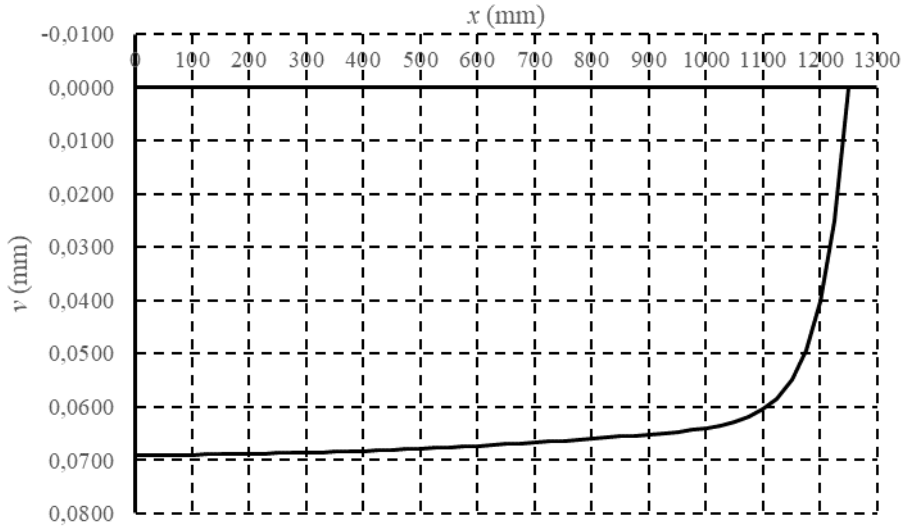

Figure 20. Deflections in the case number 2.

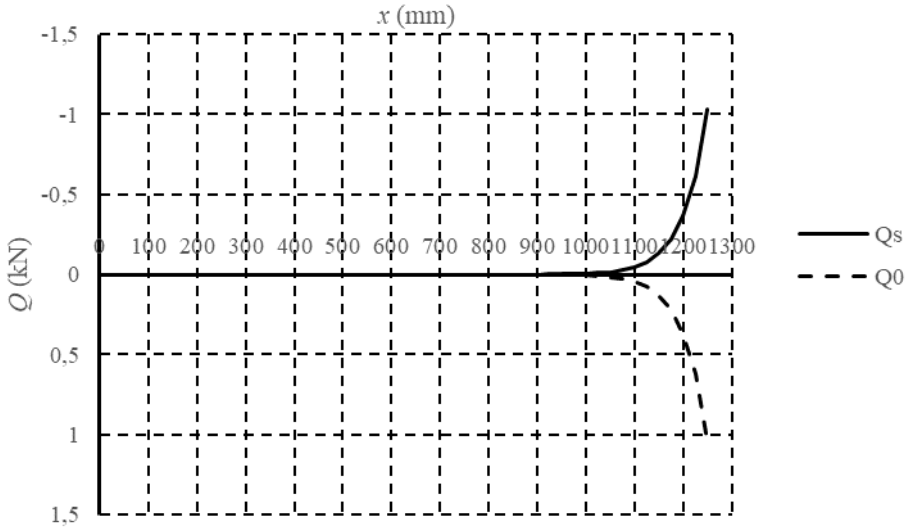

Figure 21. Shear forces in the case number 2.

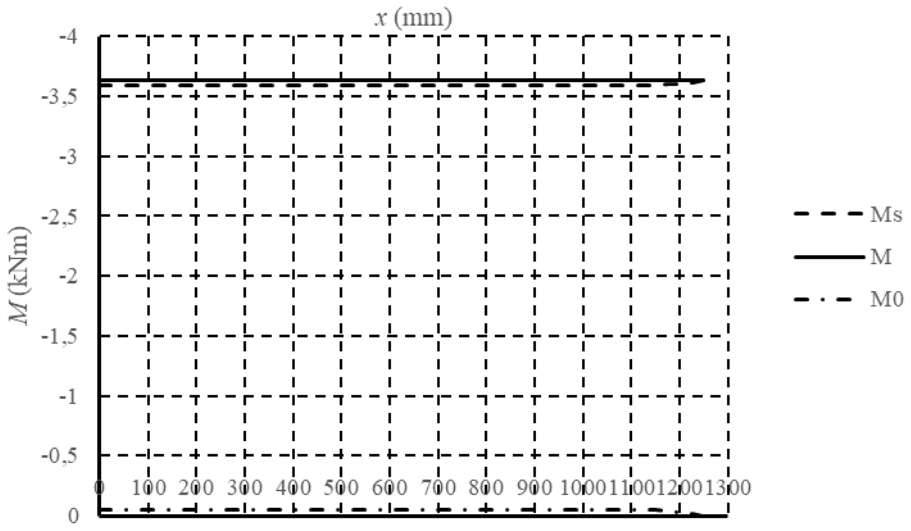

Figure 22. Moments in the case number 2.

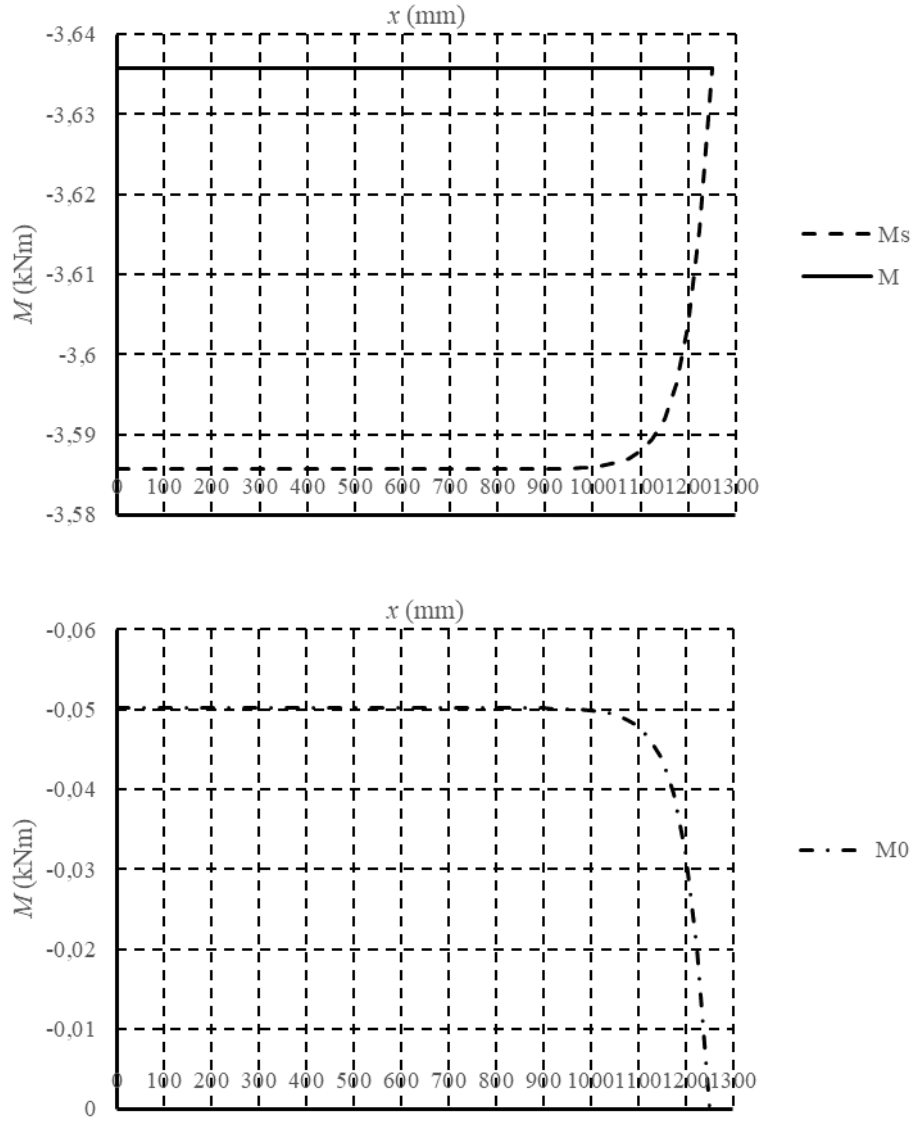

Figure 23. Moments M, M_s and M_0 in the case number 2.

The absolute maximum shear stress of the core is 0.011 MPa at the end of the beam. It is seen the high stress concentrations at the end of the beam.

The boundary conditions number 3 in Figure 6 at both ends $v = M = \gamma = 0$ lead to the following parameters

$$C_1 = 0, C_2 = \frac{\vartheta L^2}{8}, C_3 = -\frac{\vartheta}{2}. \tag{8.19}$$

Deflections are shown in Figure 24.

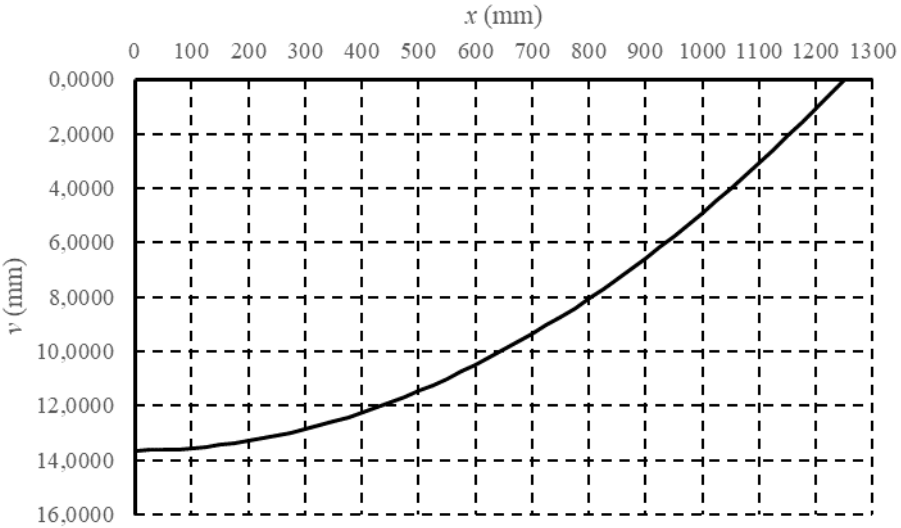

Figure 24. Deflections in the case number 3.

All shear forces are zero and the moments are constant along the beam and $-M_0 = M_s = 0.0168$ Nmm The axial stresses are much smaller than in the previous case.

The boundary conditions number 4 in Figure 6 at both ends $v = M = M_0 = 0$ lead to the following parameters

$$C_1 = \frac{\vartheta-(\vartheta_1+\vartheta_2)}{\lambda^2 \cosh \lambda L/2}, C_2 = -\frac{\vartheta-(\vartheta_1+\vartheta_2)}{\lambda^2} + \frac{\vartheta L^2}{8}, C_3 = -\frac{\vartheta}{2}. \quad (8.20)$$

Deflections and bending moments are shown in Figures 25 – 27.

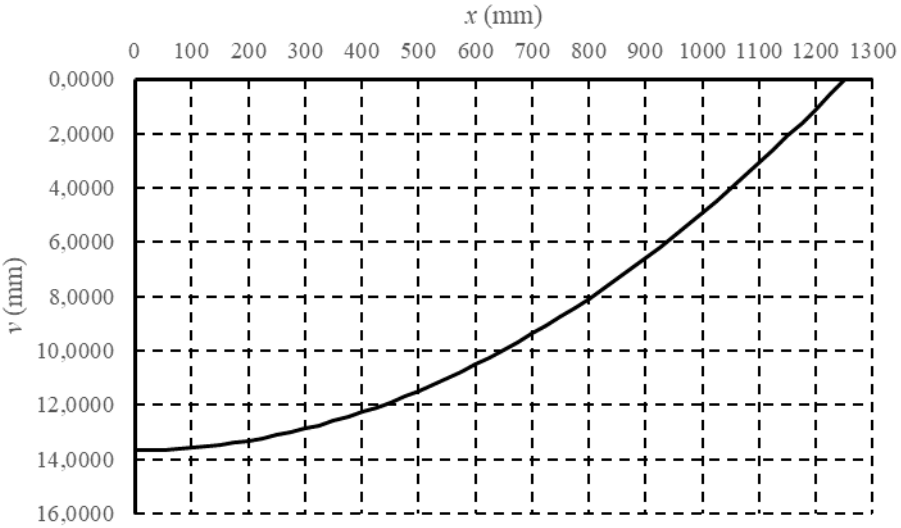

Figure 25. Deflections in the case number 4.

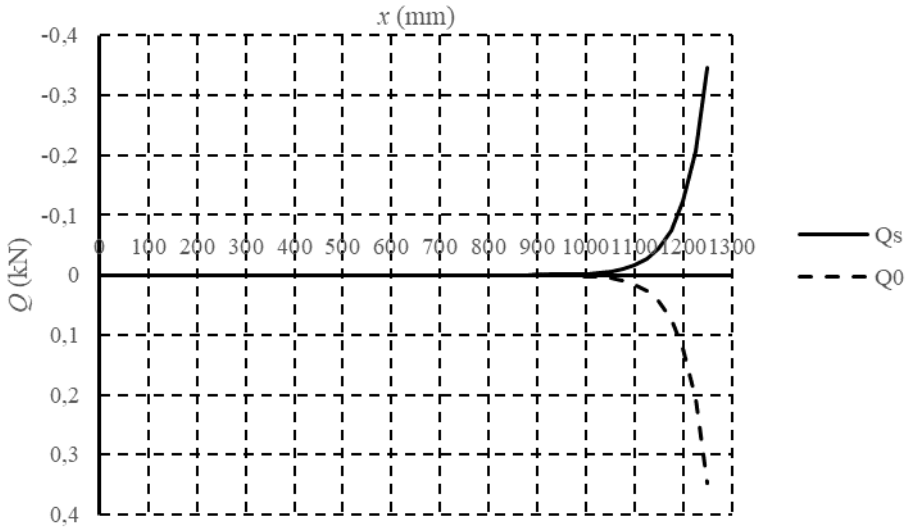

Figure 26. Shear forces in the case number 4.

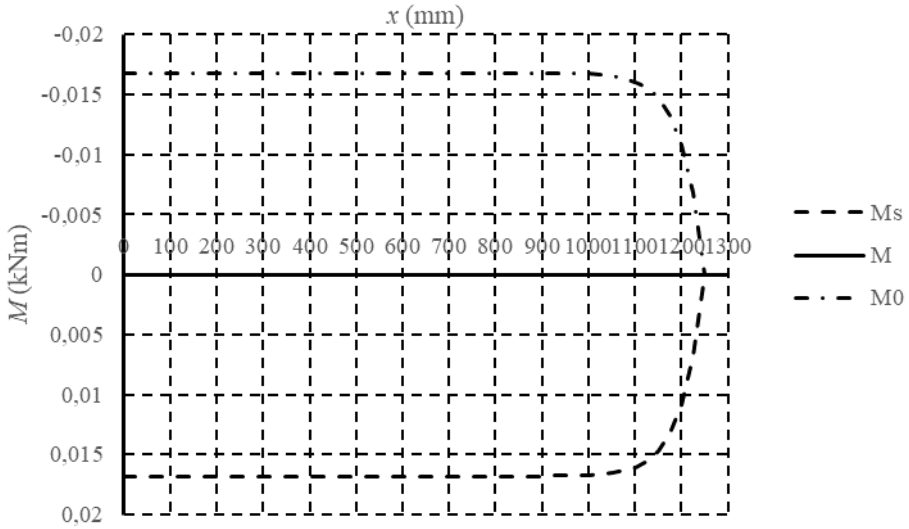

Figure 27. Bending moments in the case number 4.

The similar stress concentrations are seen as in the case number 2. However, the deflections are much larger in this case and the shear forces and the moments are smaller.

The boundary conditions number 5 in Figure 6 at both ends $Q_y = \varphi = \gamma = 0$ lead to the parameters $C_1 = C_3 = 0$ and the parameter C_2 is not defined because the free body motion of the beam is possible. Moments are same as in the case 1.

In the case of the boundary conditions number 6 in Figure 6 at both ends $Q_y = \varphi = M_0 = 0$ indicate that the parameter C_2 is not defined because the free body motion of the beam is possible. Other parameters are

$$C_1 = -\frac{\vartheta_1+\vartheta_2}{\lambda^2 \cosh\frac{\lambda L}{2}+\frac{\lambda B_0}{B_S\left(\frac{L}{2}\right)}\sinh\frac{\lambda L}{2}}, C_3 = \frac{\lambda B_0}{B_S L} C_1 \sinh\frac{\lambda L}{2}. \tag{8.21}$$

The deflections of Figure 28 are drawn using the value $C_2 = 0$. The shear forces and the moments are shown in Figures 29 – 31.

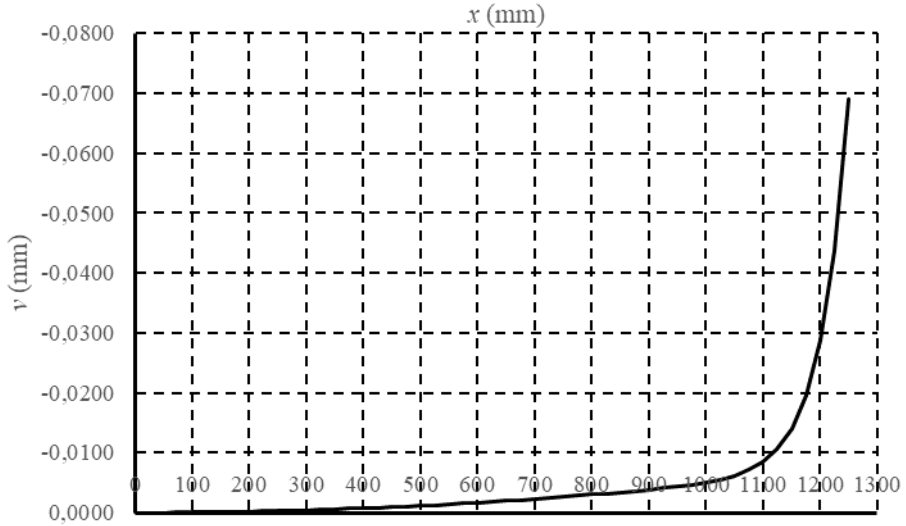

Figure 28. Deflections in the case number 6.

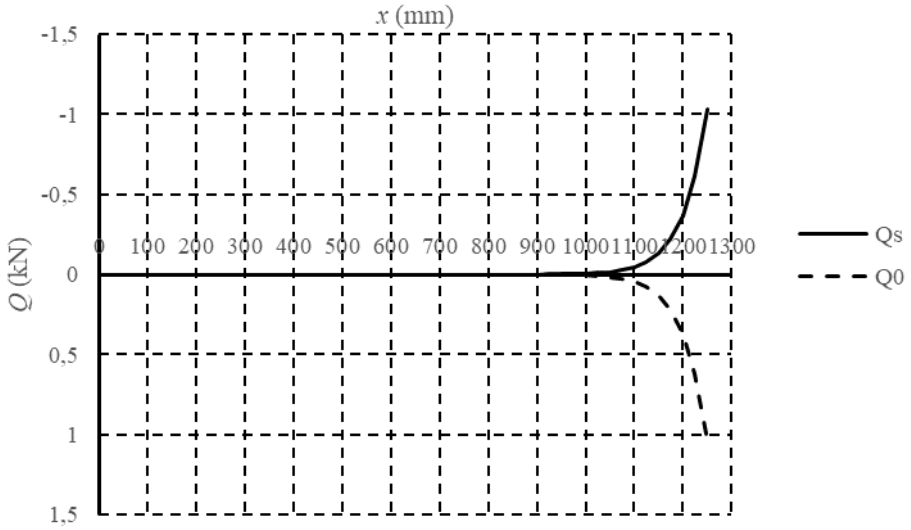

Figure 29. Shear forces in the case number 6.

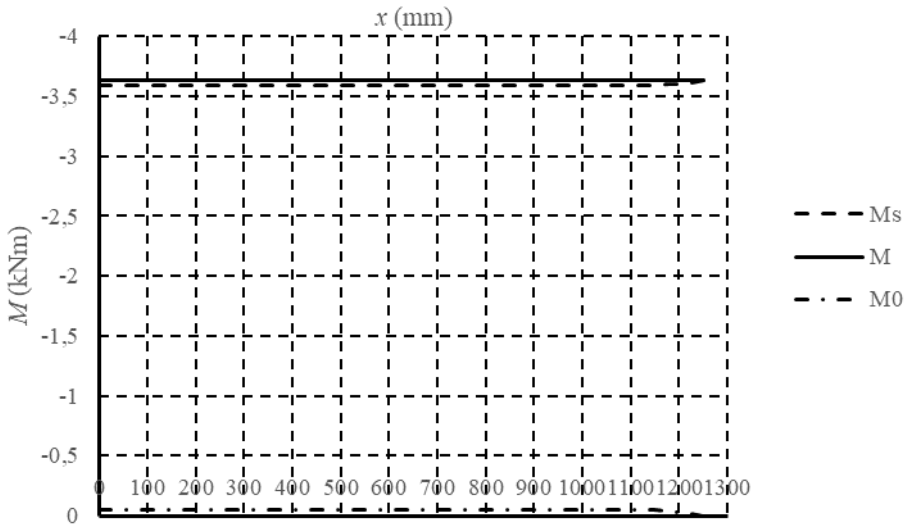

Figure 29. Bending moments in the case number 6.

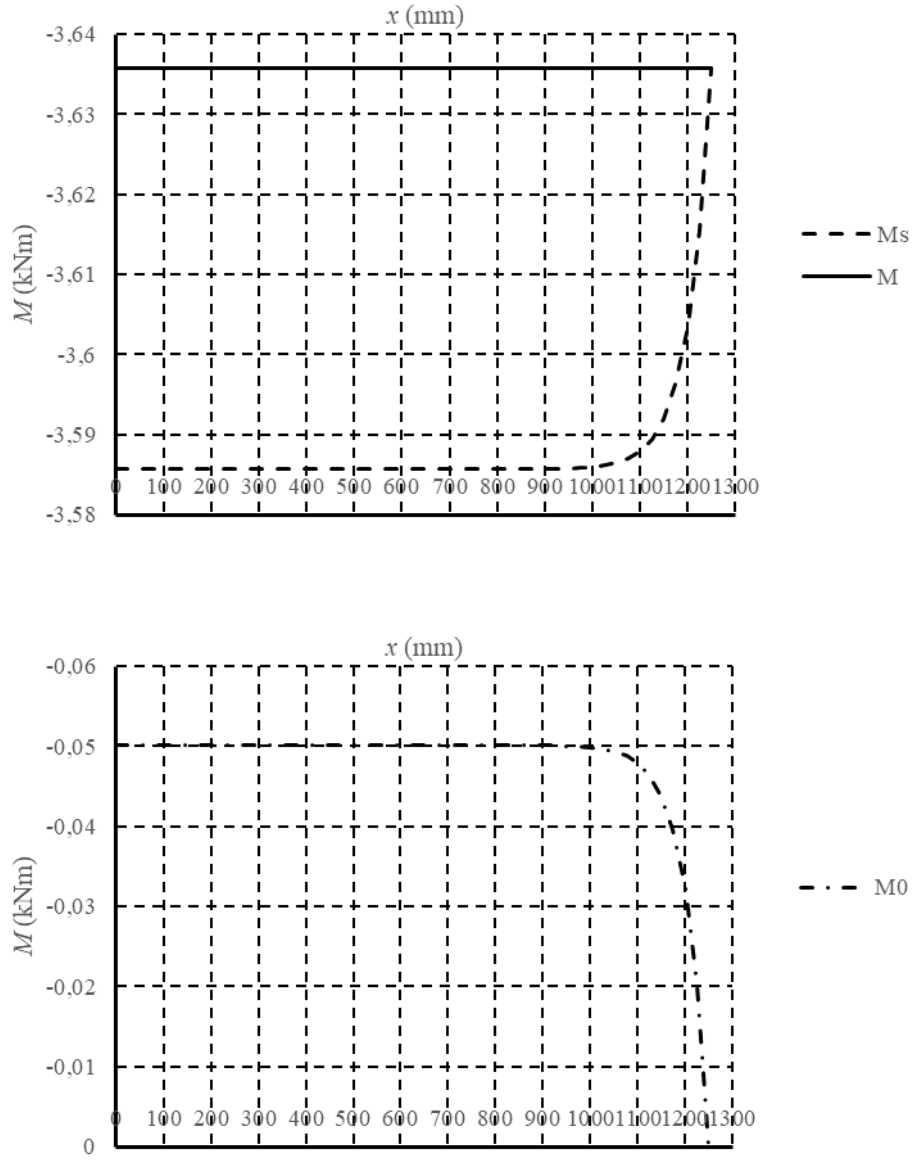

Figure 30. Bending moments M, M_s and M_0 in the case number 6.

It is seen, that the shear forces and the moments are same as in the case 2.

In the case of the boundary conditions number 7 in Figure 6 at both ends $Q_y = M = \gamma = 0$ indicate that the parameter C_2 is not defined because the free body motion of the beam is possible. Other parameters are

$$C_1 = 0, C_3 = -\frac{\vartheta}{2}. \tag{8.22}$$

The deflections in Figure 31 are drawn using the value $C_2 = 0$.

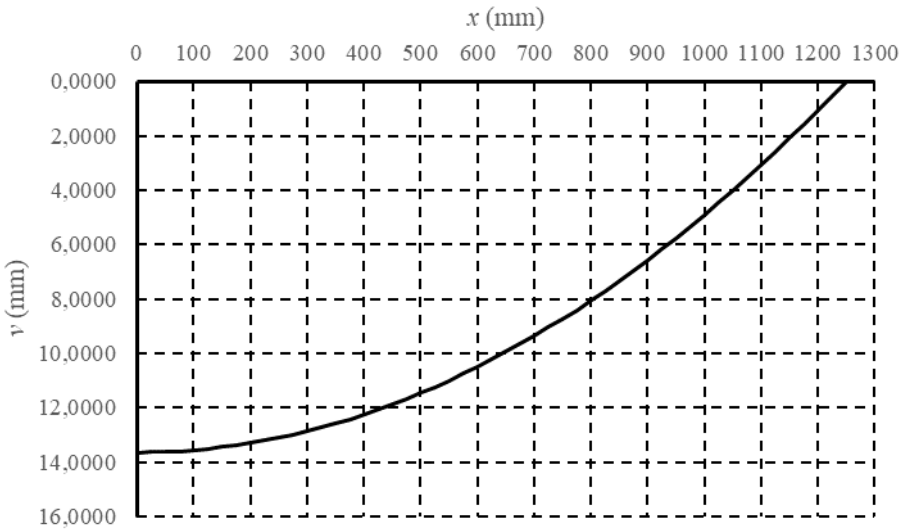

Figure 31. Deflections in the case number 7.

The bending moments are same as in the case 3.

In the case of the boundary conditions number 8 in Figure 6 at both ends $Q_y = M = M_0 = 0$ indicate that the parameter C_2 is not defined because the free body motion of the beam is possible. Other parameters are

$$C_1 = \frac{\vartheta - (\vartheta_1 + \vartheta_2)}{\lambda^2 \cosh\frac{\lambda L}{2}}, C_3 = -\frac{\vartheta}{2}. \tag{8.23}$$

The deflections in Figure 32 are drawn using the value $C_2 = 0$. The shear forces and the bending moemnts are shown in Figures 33 – 34.

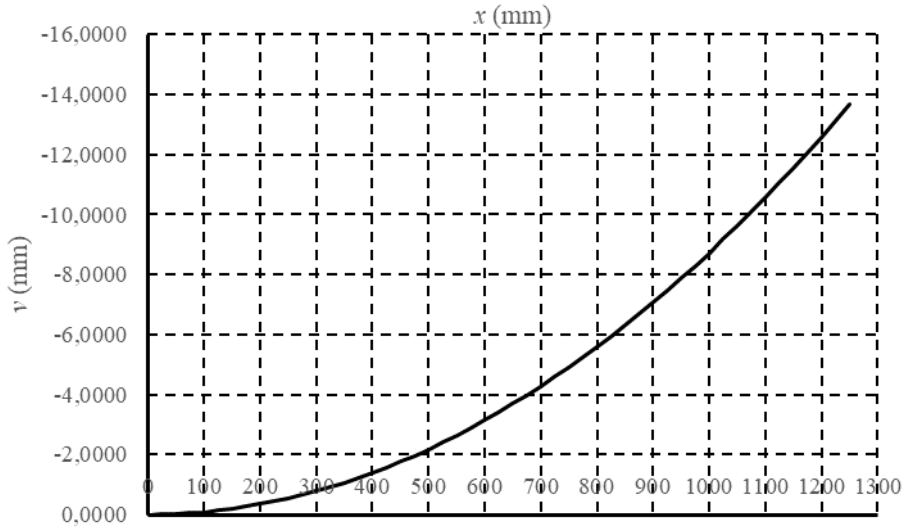

Figure 32. Deflections in the case number 8.

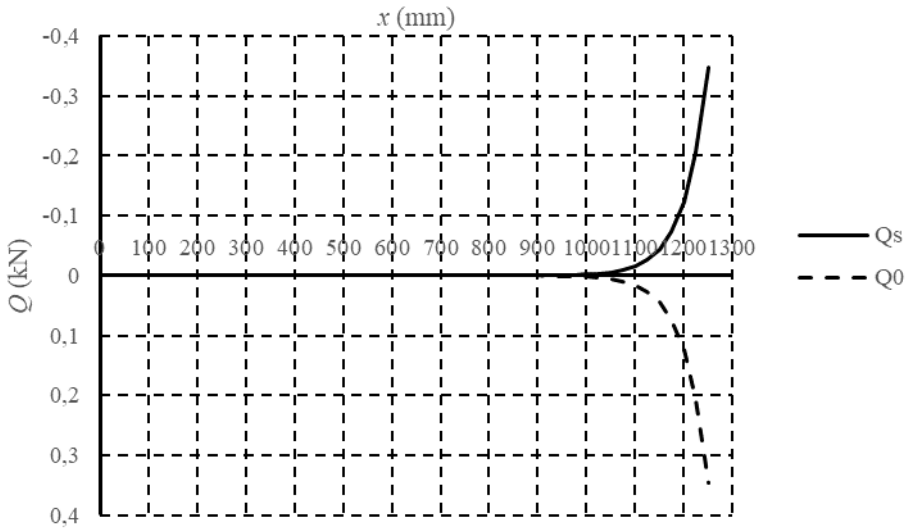

Figure 32. Shear forces in the case number 8.

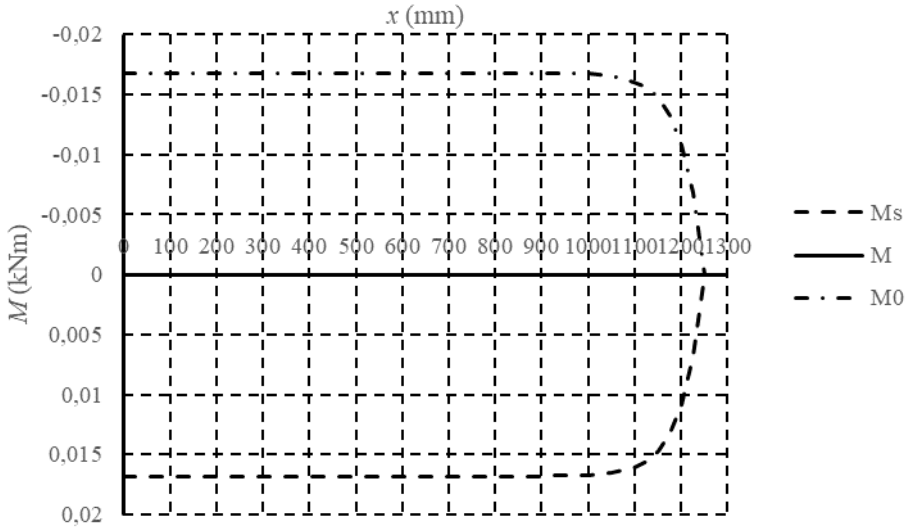

Figure 33. Bending moments in the case number 8.

Conclusions

The classical theory of layered beams is presented in details. The theory has been presented originally in 1940's to the design of composed wooden structures. Discussion is given including different definitions of the shear factor and some details of the theory. Summaries of recently presented cases of cross-laminated timber (CLT) beams and steel-timber composite beams are given including validation of the theory against experimental researches done by others. These cases include bending of the CLT beams, bending and vibration of the steel-timber composite beams and bending of the CLT beams out-of-plane with the eccentric axial load. The formulation of the theory is given for the analysis of the layered beams with temperature or moisture loading.

It is seen that the deflections and axial strains using the theory of the layered beams fit rather well to the observations in the tests, and the results being mainly at the safe side. The effects of the different shear factors were not large for the results of the CLT beams. The theory estimates well the start of the yield of the steel beam in the steel-timber composite beams and rather well the ultimate loads of the CLT beams which are loaded by the eccentric axial loads causing out-of-plane bending. The calculated fundamental structural frequencies of the steel-timber beams fitted well to the measured frequencies.

It is seen that the theory seems to be useful in estimation of the behaviour of these rather novel innovative structures. So far the theory has been used in the standards of sandwich and steel structures, but it seems to be suitable for example for possible future standards of CLT and steel-timber composite structures, as the theory was originally developed for wooden structures.

References

S. Aicher, D. Noack. Zum Einfluss des Randabschlusses bei Sandwichelementen unter Feuchtigkeits- und Temperaturbeanspruchung. *Bauingenieur* 62, 1987, 263-272.

A. Aspila, M. Heinisuo, K. Mela, M. Malaska, S. Pajunen. Elastic design of steel-timber composite beams. 2022, in progress.

E. Borgström, J. Fröbel (Eds.). *The CLT Handbook, CLT structures – facts and planning*. Swedish Wood, 2019. ISBN 978-91-983214-4-3

C. Boyer. *A History of Mathematics*. New York, John Wiley & Sons, Inc, 1968.

D. Buck, X. Wang, O. Hagman, A. Gustafsson. Bending Properties of Cross Laminated Timber (CLT) with a 45º Alternating Layer Configuration. *BioResources* 11(2): 4633-4644, 2016. DOI 10.15376/biores.11.2.4633-4644

K. Buka-Vaivade, D. Serdjuks, V. Goremikins, A. Vilguts, L. Pakrastins. Experimental verification of design procedure for elements from cross-laminated timber. *Procedia Engineering* 172: 121-1219, 2017. DOI 10.1016/j.proeng.2017.02.142

C. Ceallaigh, K. Sikora, A. Harte. The Influence of Panel lay-up on the Characteristic Bending and Rolling Shear Strength of CLT. *Buildings* 8(114), 2018. DOI 10.3390/buildings8090114

A. Chiniforush, M. Makki Alamdari, U. Dackermann, H. Valipour, A. Akbarnezhad. Vibration behaviour of steel-timber composite floors, part (1): Experimental & numerical investigation, *J Constr Steel Res* 161, 2019, 244–257.

L. Chitty. On the cantilever composed of a number of parallel beams interconnected by cross bars. *Phil. Mag.* Series 7, 38(285): 685-699, 1947.

K. Chong, K. Engen, J. Hartsock. Thermal stresses and deflection of sandwich panels. *Journal of Structural Division*, Proceedings of the ASCE 103, ST1, 1977, 35-49.

I. Christovasilis, M. Brunetti, M. Follesa, M. Nocetti, D. Vassallo. Evaluation of the Mechanical Properties of Cross Laminated Timber with Elementary Beam Theories. *Construction and Building Materials*. September 2016. DOI 10.1016/j.conbuildmat.2016.06.082

R. Clough, J. Penzien. *Dynamics of Structures*. New York, McGraw-Hill Inc, 1975.

J. Davies. Torsion-bending analysis made easy. *Proc. Instn Civ. Engrs* 2, 79, 1985, 737-747.

J. Davies. The analysis of sandwich panels with profiles faces. Proc. *Eight International Specialty Conference on Cold-Formed Steel Structures*. Department of Civil Engineering, University of Missouri-Rolla, St Luis, Nov. 11-12. 1986, 351-369.

J. Davies. *Lightweight Sandwich Construction.* Wiley, 2001.

EN 1993-1-1. Eurocode 3: Design of steel structures – Part 1-1: General – Common rules and rules for buildings. *European Committee for Standardization*. CEN, 2005.

EN 1995-1-1. Eurocode 5: Design of timber structures – Part 1-1: General – Common rules and rules for buildings. *European Committee for Standardization*. CEN, 2014.

EN 14509. Self-supporting double skin metal faced insulating panels - Factory made products – Specifications. *European Committee for Standardization*. CEN, 2013.

B. Fransson. Unsymmetrical multi-story buildings. *Chalmers University of Technology*, Department of Structural Mechanics, Publication 73:4, 1973.

S. Gagnon, C. Pirvu (Eds.). *CLT Handbook: cross-laminated timber*. Canadian Edition. 2011. ISBN 978-0-86488-547-0

J. Gluck. Lateral-load analysis of asymmetric multistory structures. *Journal of Structural Division*, Proceeding of the ASCE 96(ST2), 1970, 317-333.

H. Granholm. Om sammansatta balkar och pelare med särskild hänsyn till spikade träkonstruktioner (On composite beams and columns with particular regard to nailed timber structures). *Transactions of Chalmers University of Technology*, No. 88. Göteborg, 1949.

A. Hassanieh, H. Valipour, M. Bradford. Experimental and numerical study of steel-timber composite (STC) beams. *J Constr Steel Res* 122, 367-378, 2016.

A. Hassanieh, H. Valipour, M. Bradford. Experimental and numerical investigation of short-term behaviour of CLT-steel composite beams. *Eng Struct* 144, 43-57, 2017.

A. Hassanieh, A. Chiniforush, H. Valipour, M. Bradford. Vibration behaviour of steel-timber composite floors, part (2): evaluation of human-induced vibrations. *J Constr Steel Res* 158, 2019. 156-170.

M. He, X. Sun, Z. Li, W. Feng. Bending, shear, and compressive properties of three- and five-layer cross-laminated timber fabricated with black spruce. *Journal of Wood Science* 66:38, 2020. DOI 10.1186/s10086-020-01886-z

M. Heinisuo, S. Malmi, A. Möttönen. Exact finite element method for sandwich beams. *Composite Structures* 4(1), Elsevier Applied Science, 1987, 1.536-1.554.

M. Heinisuo, An exact finite element technique for layered beams. *Computers & Structures* Vol 30. No. 3. 615-622, 1988.

M. Heinisuo. Exact Finite Element Method for Layered Beams. *Publications 56, Tampere University of Technology*, Tampere, 1989.

M. Heinisuo, S. Pajunen. CLT beam analysis using classical elastic theory of layered beams. *Rakenteiden Mekaniikka* 10(4), 2021, 143-171.

N. Hoff, S. Mautner. Bending and buckling of sandwich beams. *Journal of the Aeronautical Sciences* 15(12): 707-720, 1948.

W. Howson, F. Williams. Natural frequencies of frames with axially loaded Timoshenko members. *Journal of Sound and Vibration* 26(4), 1973, 503-515.

Z. Huang, D. Huang, Y. Chui, Y. Shen, H. Daneshvar, B. Sheng, Z. Chen. Modeling of Cross-Laminated Timber (CLT) panels loaded with combined out-of-plane bending and compression. *Engineering Structures*, *250*, 2022, 113335.

R. Itani, G. Hiremath. Partial composite action in diaphragms. *Journal Engineering Mechanics Division*. Proceedings of the ASCE 106(EM4): 739-751, 1980.

E. Karacabeyli, B. Douglas. *CLT Handbook: cross-laminated timber*. US Edition. 2013. ISBN 978-0-86488-553-1

H. Kreuzinger. Flächentragverke – Platten, Scheiben und Schalen – Berechnungsmethoden und Beispiele. *Fachverlag Holz*. Dusseldorf, 1999.

H. Langhaar. *Energy Methods in Applied Mechanics*. New York, John Wiley & Sons, Inc, 1962.

E. Lindelöf. *Johdatus korkeampaan analyysiin*. Porvoo, Werner Söderström Oy, 1956. (in Finnish)

C. Loss, B. Davison. Innovative composite steel-timber floors with prefabricated modular components. *Eng Struct* 132, 2017, 695-713.

S. Malmi. Kaksipaarteisen Sandwich-palkin tarkka dynaaminen analyysi elementtimenetelmällä (Exact dynamic analysis of two-faced sandwich beam using finite element analysis). *Master thesis. Tampere University of Technology*, Tampere, 1987. (in Finnish)

G. Monforton. Stiffness matrix for sandwich beams with thick anisotropic laminated faces. *Computers & Structures* 10(3), 1979, 547-551.

K. Möhler. Über das Tragverhalten von Biegeträgern und Druckstäben mit zusammengesetzten Querschnitten und nachgiebigen Verbindungsmitteln. *Habilitation*: Technische Universität Karlsruhe, Germany, 1956.

A. Möttönen. Kaksipaarteisen sandwich-palkin tarkka elementtimenetelmä taivutuspuristuksessa ja lämpökuormituksessa (Exact finite element method of two-faced sandwich beam in bending/compression and in thermal loading). *Master thesis. Tampere University of Technology*. Tampere, 1987. (in Finnish)

H. Parland. Yhdistettyjen puukannattajien lujuus (Strength of composite wooden structures). Helsinki, 1946. (in Finnish)

H. Parland. Rakennustatiikan sovellutuksia (Applications of building static). *Tampere University of Technology*, Tampere, 1972. (in Finnish)

P. Pleskov. Teoriia rascheta dereviannykh sostavnnykh sterzhnei (Theoretical studies of composite wood structures). Moscow, 1952. (in Russia)

R. Rosman. Die statische Berechnung von Hochhauswänden mit Öffnunsreihen. *Bauingenieur-Praxis*. Heft 65, Berlin, Verlag von Wilhelm Ernst & Sohn, 1965.

G. Ruan, H. Xiong, J. Chen. Bending and Rolling Shear Properties of Cross-Laminated Timber Fabricated with Canadian Hemlock. *SDHM*. Vol 13(2): 227-246, 2019. DOI 10.32604/shdm.2019.04743

G. Schickhofer, T. Bogensperger, T. Moosbrugger (Eds.). *BSPhandbuch: Holz-Massivbauweise in Brettsperrholz – Nachweise auf Basis des neuen europäischen Normenkonzepts*. Verlag der Technischen Universität Graz. Graz, 2010.

K. Schwarze. Numerische Methoden zur Berechnung von Sandwichelementen. *Stahlbau* 12, 1984, 363-370.

K. Stamm, H. Witte. *Sandwichkonstruktionen. Berechnung, Fertigung, Ausführung*. Springer-Verlag, Wien, New York, 1974.

K. Stamm. Sandwichelemente mit metallischten Deckschihten als Dachbautafeln im Bauwesen. *Stahlbau* 53, 8, 1984, 231-236.

M. Sultan, B. Di Leonardo. Structural performance evaluation of CLT wall-segment/columns under centric and eccentric loadings, *A report to NRC*, Canada, Report No. A1-005432.3, June 30, 2015.

E. Thompson, J. Goodman, M. Vanderbilt. Finite element analysis of layered wood systems. *Journal of Structural Division*. Proceedings of the ASCE 101(ST12): 2659-2671, 1975.

S. Timoshenko. On the correction factor for shear of the differential equation for transverse vibrations of bars of uniform cross-section. *Phil. Mag.* 41: 744-746, 1921.

F. Williams, W. Wittrick. An automatic computational procedure for calculating natural frequencies of skeletal structures. *Int. J. Mech. Sci.* 12, 1970, 781-791.

C. Zhang, G. Lee, F. Lam. Connection and performance of two-way CLT plates. *UBC TEAM Report: TEAM 2017-08, University of British Columbia*, Vancouver, Canada, 2018.

Appendix A. Solution of the cubic equation

Consider the equation

$$\lambda^3 + 3p\lambda + 2r = 0 \tag{A1}$$

Viete discovered that the substitution $\bar{\lambda}^2 + \bar{\lambda}\lambda = p$ transforms the cubic equation into a quadratic equation in the variable $\bar{\lambda}^3$. The sign of the discriminant of the resulting equation is a very important factor when solving the roots of the original equation. Discriminant D is

$$D = r^2 + p^3 \tag{A2}$$

Three distinct cases can be considered for the roots of the cubic equation:

- $D > 0 \Rightarrow$ one real and two imaginary roots,
- $D = 0 \Rightarrow$ two or three equal real roots,
- $D < 0 \Rightarrow$ three different real roots.

The real root for the case $D > 0$ is:

$$\lambda = \frac{p}{\sqrt[3]{s}} - \sqrt[3]{s}$$
$$s = r \pm \sqrt{r^2 + p^3} \tag{A3}$$

If $D < 0$ then the real roots, provided, that $p < 0$, are:

$$\lambda_1 = 2\sqrt{-p}\cos\frac{\phi}{3} \tag{A4}$$

$$\lambda_2 = -2\sqrt{-p}\cos\frac{\pi - \phi}{3} \tag{A5}$$

$$\lambda_3 = -2\sqrt{-p}\cos\frac{\pi + \phi}{3} \tag{A6}$$

where:

$$\phi = \overline{arccos}\left(-\frac{r}{w}\right) \tag{A7}$$

$$w = \sqrt{-p^3} \tag{A8}$$